Carbon Neutralization

WILEY

REVIEW OPEN ACCESS

Biomass-Derived Carbon Photocatalysts for Organic Pollutant Degradation: Strategies and Perspectives

Jagadis Gautam[1,2] | Amol M. Kale[3] | Jishu Rawal[3] | Pooja Varma[4] | Seung Jun Lee[4] | Seul-Yi Lee[1,2] | Soo-Jin Park[1,2]

[1]Department of Mechanical Engineering, College of Engineering, Kyung Hee University, Yongin, South Korea | [2]Department of Convergent Biotechnology and Advanced Materials Science, Kyung Hee University, Yongin, South Korea | [3]Department of Chemistry, Inha University, Incheon, Republic of Korea | [4]Department of IT-Energy Convergence (BK21 Four), Korea National University of Transportation, Chungju, Republic of Korea

Correspondence: Seung Jun Lee (sjlee@ut.ac.kr) | Seul-Yi Lee (leesy1019@gmail.com) | Soo-Jin Park (soojinpark@khu.ac.kr)

Received: 24 September 2025 | **Revised:** 21 November 2025 | **Accepted:** 11 December 2025

Funding: Commercialization Promotion Agency for R&D Outcomes (COMPA) grant funded by the Korea government (Ministry of Science and ICT), Grant/Award Number: RS-2025-2311658; Korea government (MSIT), Grant/Award Number: 2023R1A2C1004109

Keywords: biomass-derived carbon nanostructures | photocatalysis | pollutant degradation | surface functionalization

ABSTRACT

The accumulation of persistent organic pollutants (POPs) in aquatic systems poses severe environmental and health risks, underscoring the need for sustainable, efficient remediation technologies. Biomass-derived carbon materials have emerged as cost-effective photocatalysts owing to their high surface area, tunable electronic structure, and excellent charge transport properties. This review summarizes recent progress in their synthesis, structural design, and surface modification for photocatalytic degradation of organic pollutants. Emphasis is placed on key mechanisms such as reactive oxygen species (ROS) generation, band gap tuning, and interfacial charge separation, as well as performance-enhancing strategies including heteroatom doping, heterojunction formation, and hybrid integration for improved visible-light activity. The dual functionality of these materials in adsorption and photocatalysis is also highlighted, revealing synergistic pollutant removal pathways. Finally, critical challenges related to scalability, stability, and reproducibility are discussed, along with future perspectives for translating biomass-derived carbon photocatalysts from laboratory research to practical environmental applications.

1 | Introduction

Rapid urbanization, accompanied by escalating domestic and industrial water demands, has placed unprecedented stress on global freshwater reserves. This mounting pressure has significantly intensified water-related challenges, particularly the contamination and deterioration of aquatic ecosystems. One of the primary drivers of this environmental degradation is the unchecked release of toxic pollutants—including heavy metals, pesticides, synthetic dyes, surfactants, and pharmaceutical residues—by industrial facilities and municipal wastewater systems. These contaminants not only deteriorate water quality but also pose serious threats to public health and the integrity of aquatic ecosystems [1–3]. Chronic exposure to heavy metals such as zinc, copper, nickel, chromium, mercury, arsenic, cadmium, and lead, alongside a broad spectrum of persistent organic pollutants (POPs)—including phenols, chlorinated phenols, polycyclic aromatic hydrocarbons (PAHs), azo dyes, and endocrine-disrupting compounds—has been linked to numerous adverse health effects. These include carcinogenesis, neurotoxicity, reproductive dysfunction, and hormonal imbalances in both humans and aquatic organisms [4, 5]. Industrial sectors such as textiles, pharmaceuticals, petrochemicals, and agriculture are particularly notorious for discharging complex and often synergistically toxic mixtures of volatile

Jagadis Gautam and Amol M. Kale contributed equally to this study.

organic compounds (VOCs), dyes, and other chemical residues into natural water bodies, thereby aggravating concerns related to ecotoxicity, bioaccumulation, and long-term ecological damage [6, 7]. The global dye industry alone contributes significantly to aquatic pollution, with an estimated annual production of over 700,000 metric tonnes and more than 100,000 synthetic dye variants introduced since the advent of industrial dye synthesis in 1856. A significant proportion of these dyes are non-biodegradable, aromatic, and chromophoric, enabling them to persist in aquatic environments for extended durations. Their presence inhibits light penetration, disrupts aquatic photosynthesis, and induces oxidative stress in aquatic biota [8]. To address these complex water contamination issues, a range of physicochemical and biological remediation strategies have been investigated. These include ozonation, biosorption, ion exchange, catalytic combustion, chemical precipitation, electrochemical oxidation, and advanced oxidation processes (AOPs) like photocatalysis [9–11]. Among these, photocatalysis has emerged as the most promising and sustainable option. Its advantages include low energy requirements, environmental compatibility, rapid degradation kinetics, and the ability to achieve complete mineralization of organic and inorganic pollutants under mild conditions. The core mechanism involves the excitation of semiconductor photocatalysts under light irradiation, generating reactive oxygen species (ROS)—such as hydroxyl ($^{\bullet}OH$) and superoxide ($O_2^{\bullet-}$) radicals—which actively break down pollutants. Semiconductor metal oxides, including TiO_2, ZnO, ZnS, CdS, and Fe_2O_3, have been extensively studied due to their inherent stability, non-toxicity, and low cost. Among these, ZnO has garnered particular attention as a viable alternative to TiO_2, owing to its high exciton binding energy (~60 meV), superior electron mobility, thermal and chemical robustness, and excellent quantum yield [12, 13]. Furthermore, ZnO is both biocompatible and environmentally benign, with FDA-approved applications in antimicrobial products, underscoring its selectivity toward microbial targets while remaining safe for human use. However, despite these promising attributes, ZnO-based photocatalysts face several operational limitations. Their wide bandgap (~3.37 eV) restricts their photoactivation to the ultraviolet (UV) region, which constitutes only about 3%–5% of the solar spectrum. Moreover, ZnO is susceptible to photo corrosion, agglomeration, and rapid recombination of photogenerated electron-hole pairs, all of which reduce its photocatalytic efficiency and long-term operational stability in real-world water treatment systems [14, 15].

To overcome these challenges and harness the full potential of solar energy, recent research has increasingly focused on the development of hybrid photocatalytic systems incorporating biomass-derived carbon nanostructures (BMCNSs) as functional supports, sensitizers, or co-catalysts. BMCNSs are engineered from renewable and abundantly available biomass sources, ranging from agricultural and forestry residues to urban organic waste, offering a sustainable route to carbonaceous nanomaterials with exceptional structural and chemical versatility (Figure 1). BMCNSs exhibit numerous advantages over their fossil fuel-based counterparts, including low cost, sustainable availability, high carbon content, and ease of processing [16, 17]. Notably, biomass waste is emerging as a critical

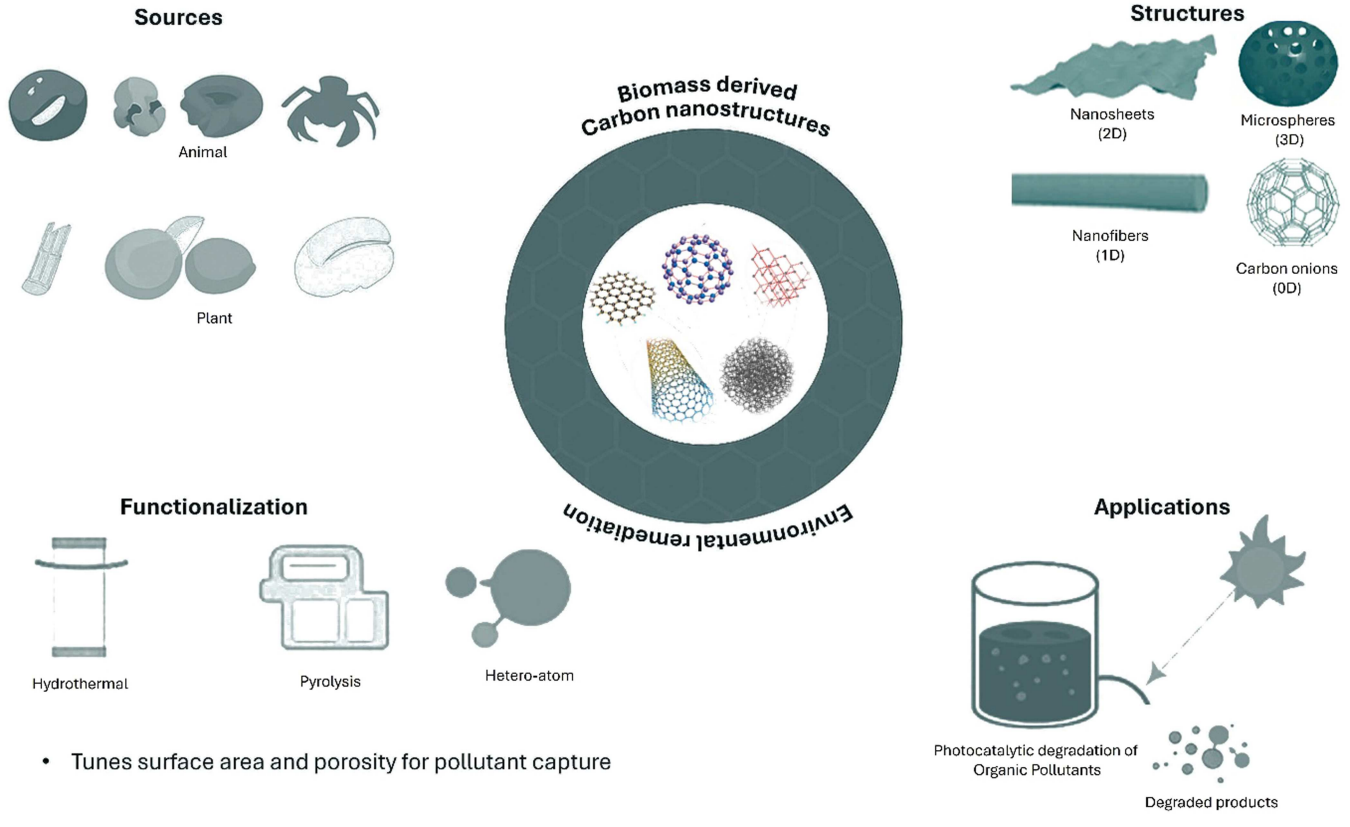

FIGURE 1 | Schematic of biomass-derived carbon nanostructures (BMCNSs) showing sources, functionalization methods, and structures for enhanced photocatalytic degradation of organic pollutants (OPs).

carbon source due to its environmental and economic benefits. For instance, the global leather industry generates approximately 8–9 million tonnes of hides annually, yielding about 1.4 million tonnes of protein-rich solid waste. Rather than being discarded through landfilling or incineration—methods that contribute to pollution and occupy valuable land—this waste can be upcycled into functional carbon materials, thereby reducing environmental burden while generating value-added products. The inherent diversity of molecular structures and the presence of heteroatoms (e.g., nitrogen, sulfur, phosphorus) in biomass feedstocks enable the synthesis of carbon materials with tailored properties such as tunable porosity, enhanced surface chemistry, and improved electrical conductivity. These characteristics are instrumental in designing multifunctional carbonaceous nanostructures—such as carbon dots, carbon aerogels, and hierarchical porous carbons—that serve a wide array of applications, including environmental remediation, energy storage, sensing, and bioimaging. In the context of photocatalysis, the integration of BMCNSs with semiconductor materials provides a synergistic platform to address the key drawbacks of conventional photocatalysts. Specifically, BMCNSs enhance visible-light absorption, facilitate charge separation and transport, and increase the adsorption capacity for pollutant molecules. Moreover, their heteroatom-doped frameworks can introduce localized energy states that narrow the bandgap and promote photocatalytic activity under visible light [18–20].

This review emphasizes the critical role of functionalized BMCNSs in enhancing the photocatalytic degradation of OPs. Functionalization techniques—ranging from heteroatom doping to surface oxidation and polymer grafting—have been employed to fine-tune surface energy, modify wettability, and enable specific molecular interactions with target contaminants. These modifications not only improve the photocatalytic reactivity but also allow BMCNSs to be incorporated into composite systems such as mixed matrix membranes (MMMs). Such hybrid systems exhibit improved permeability, antifouling behavior, hydrophobicity, and antibacterial performance, making them highly suitable for advanced water purification applications. This implies a transformative advancement of BMCNSs in the field of photocatalysis. Their sustainable origin, functional versatility, and ability to augment semiconductor performance position them as next-generation materials for water treatment technologies. Continued innovation in their functionalization and integration strategies holds promise for developing highly efficient, scalable, and eco-friendly photocatalytic systems aimed at mitigating organic pollution and safeguarding aquatic environments.

2 | Overview of Organic Pollutants and Their Photocatalytic Degradation Mechanisms

Agrochemical and pharmaceutical pollutants, including pesticides, herbicides, and drug residues, represent major organic contaminants in aquatic systems. These pollutants often originate from petroleum-based hydrocarbons (e.g., benzene, toluene), industrial chemicals (e.g., PCBs, dioxins), persistent pesticides (e.g., DDT, atrazine), as well as phenolic compounds, dyes, and pharmaceutical byproducts [21]. Their accumulation in water bodies poses severe risks to aquatic life, disrupts ecosystems, and may induce carcinogenic, mutagenic, or endocrine-disrupting effects in humans. The persistence of these OPs depends on their chemical structure, solubility, and environmental degradation pathways. Herbicide-based OPs (e.g., glyphosate, 2,4-D) are moderately persistent due to partial biodegradability in soil and water, with reported half-lives ranging from days to a few weeks under aerobic conditions [22]. Industrial chemical-based OPs (e.g., dioxins, PCBs) are highly persistent owing to their hydrophobicity, resistance to microbial degradation, and bioaccumulative potential, resulting in long-term ecological persistence [23]. Similarly, pharmaceutical-based OPs (e.g., diclofenac, clofibric acid) generally exhibit minimal to moderate persistence; although some are partially biodegradable, their continuous introduction via wastewater maintains detectable environmental concentrations [24]. Petroleum hydrocarbon-based OPs (e.g., benzene, toluene) are moderately persistent, capable of aerobic biodegradation but prone to accumulation in sediments and biofilms, thereby prolonging their environmental presence [25]. Phenolic compounds (e.g., BPA, catechol) demonstrate moderate persistence, as some undergo microbial or photodegradation, yet widespread industrial discharge sustains their environmental levels [26]. Textile dye-based OPs (e.g., rhodamine B, crystal violet) are moderately persistent due to complex aromatic structures that resist conventional degradation pathways [27], whereas pesticide-based OPs (e.g., DDT, atrazine) show high persistence because of chemical stability, low water solubility, and strong sorption to sediments, leading to long-term environmental contamination [28]. Addressing these pollutants requires advanced treatment strategies, with photocatalysis emerging as a promising approach capable of efficiently degrading complex organic compounds in wastewater, thereby promoting environmental safety and sustainable water quality [29]. This light-driven process further enhances the breakdown efficiency of persistent OPs. Table 1 summarizes key pollutants, their sources, and associated ecological and human health impacts.

The photocatalytic degradation of OPs operates through a light-induced redox mechanism involving strong oxidizing (h^+) and reducing (e^-) species generated on the surface of semiconductor photocatalysts under UV or visible light irradiation. This process initiates when photons with energy equal to or greater than the bandgap of the semiconductor are absorbed, as illustrated in Figure 2a [30, 31]. Upon absorption, electrons in the valence band (VB) are excited to the conduction band (CB), leaving behind positively charged holes in the VB, thus generating electron-hole (e^-/h^+) pairs. These photogenerated charge carriers migrate to the surface of the photocatalyst, where they participate in oxidation and reduction reactions. Electrons in the CB can reduce molecular oxygen (O_2) to form superoxide radicals ($^{\bullet}O_2^-$), while holes in the VB oxidize surface-adsorbed water (H_2O) or hydroxide ions (OH^-) to generate highly reactive hydroxyl radicals ($^{\bullet}OH$). Both species are potent oxidants capable of degrading a broad range of OPs into benign end-products such as CO_2 and H_2O [32]. The key surface reactions are represented as follows [33]:

$$\text{Photocatalyst} + h\nu \rightarrow \text{Photocatalyst}(e^- + h^+).$$

TABLE 1 | Summary of various OPs, including their examples, sources, impacts on aquatic and human health, and environmental persistence.

Category of OPs	Examples	Origin	Influence on environment	Influence on human health	Persistence of OPs
Herbicide-based OPs	Metolachlor, glyphosate, cholridazon, 2,4-D, nicosulfuron, etc.	From weed control and agricultural crop spraying	Marine life poisoning and eutrophication	Extremely cancer-causing substances	Moderately
Industrial Chemical-based OPs	Dioxins, polycyclic aromatic hydrocarbons, nonylphenol, nonylphenol ethoxylates, polychlorinated biphenyls, etc.	In the electronics and chemical industries, waste	Chronic in ecological systems, as well as bioaccumulation	Carcinoma and immune function impairment	Extremely high
Pharmaceutical-based OPs	Clofibric acid, telmisartan, ceftriaxone, diclofenac, etc.	From medical and household wastewater	The disruption of underwater fecundity and the development of resistance to antibiotics	Chronic consequences for health and imbalances in hormones	Minimal to moderate levels
Petroleum hydrocarbon-based OPs	Toluene, benzene, chlorobenzene, xylene, etc.	From industrial waste, oil spills, etc.	Smothering environments and contaminating aquatic life	Neurotoxic and cancer-causing	Moderately
Phenolic compound OPs	Bisphenol A (BPA), phenol, creosotes, cresols, chlorophenols, catechols, pentachlorophenol, etc	In the chemical and plastic manufacturing industries, waste	Detrimental to aquatic ecosystems	Endocrine disturbances and the probability of developing cancer	Moderately
Textile dye-based OPs	Rhodamine B (RhB), methylene blue (MB), Congo red (CR), methyl orange (MO), safranin O (SO), crystal violet (CV) etc.	In the dyeing and textile industries, waste	Restrict sunlight penetration, which is harmful to fauna and plants	Deadly cancer-causing compounds cause discomfort in the skin as well as the eyes	Moderately
Pesticide-based OPs	Atrazine, DDT, endosulfan, propiconazole, imidacloprid, thiamethoxam, etc.	From agricultural crop pest control	Injure aquatic creatures and interfere with habitats	Cancer-causing, endocrine attackers	Higher

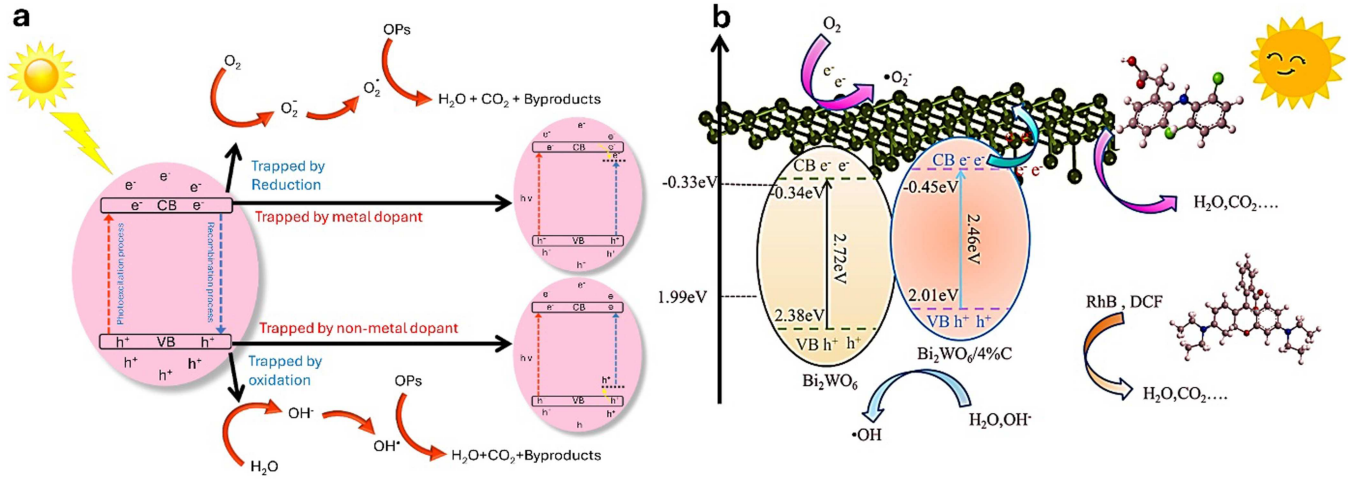

FIGURE 2 | (a) Schematic diagram illustrating the basic concept of OP photocatalytic oxidation. (b) Illustration of the BWO/4%C catalyzed pathway of photocatalytic degradation of OPs. Reproduced with permission from Reference [34], Copyright 2024, Elsevier.

$$e_{CB}^- + O_2 \rightarrow {}^{\bullet}O_2^- \quad (1)$$

$${}^{\bullet}O_2^- + H^+ \rightarrow HO_2^{\bullet} \quad (2)$$

$$h_{VB}^+ + H_2O \rightarrow H^+ + {}^{\bullet}OH \quad (3)$$

$$h_{VB}^+ + OH^- \rightarrow {}^{\bullet}OH \quad (4)$$

$$OPs + e_{CB}^-/h_{VB}^+ \rightarrow \text{redox outcomes} \quad (5)$$

$$OPs + {}^{\bullet}OH \rightarrow \text{degradation outcomes} \quad (6)$$

The photocatalytic oxidation mechanism is illustrated in Figure 2a, while Figure 2b presents the pathway proposed by Zhang et al. for the degradation of OPs using biomass-derived BWO/4%C. In this system, the incorporation of biomass-derived carbon (C) into Bi_2WO_6 (BWO) not only enhances pollutant adsorption but also facilitates efficient electron transfer and delivery, thereby accelerating charge separation between photogenerated electrons and holes. As a result, under visible-light irradiation, BWO/4%C achieved remarkable degradation efficiencies—97.27% of RhB within 50 min and 96.19% of diclofenac within 120 min. The superior performance of BWO/4%C is largely attributed to its enlarged specific surface area (33.51 m^2/g), which increases the number of active sites available for contaminant interaction. Complementary UV–Vis DRS analysis revealed that the introduction of biomass carbon narrowed the band gap of BWO, thus extending its response into the visible-light region. Additionally, the strong electron transfer ability of biomass C significantly promoted charge separation efficiency in BWO. Free radical trapping experiments further verified that photogenerated holes (h^+) and superoxide radicals (${}^{\bullet}O_2^-$) serve as the dominant reactive species driving the degradation process. Moreover, the recyclability tests demonstrated excellent stability, as the RhB degradation rate consistently remained above 90% after five consecutive cycles. Taken together, these findings highlight that biomass-derived BWO/4%C composites integrate high adsorption capacity, efficient charge transfer, and robust stability, offering a promising strategy for designing advanced nano-photocatalysts for wastewater remediation [34].

The efficiency of the photocatalytic course is influenced by several factors, including the bandgap energy of the photocatalyst, which determines its light absorption capability, especially in the visible range [35, 36]. However, a major challenge in photocatalysis is the recombination of photogenerated e^-/h^+ pairs, which reduces the number of reactive species available for pollutant degradation. Additionally, the limited interaction between photocatalyst surfaces and organic contaminants—often due to the absence of functional groups—further hampers performance. Studies using surface characterization techniques and computational modeling have shown that intermediate species formed during partial degradation can deactivate photocatalysts, limiting their long-term usability [37, 38]. To overcome the inherent limitations of conventional photocatalysts—such as wide band gaps and rapid electron–hole recombination—extensive efforts have focused on bandgap engineering and surface modification strategies. A particularly promising approach involves integrating semiconductor photocatalysts with BMCNS synthesized via biomass pyrolysis. These carbon-rich materials serve dual roles: as electron acceptors and support matrices, facilitating efficient charge separation, prolonging the lifetime of charge carriers, and substantially improving photocatalytic performance under visible light. BMCNS, especially those incorporating metal oxides or derived from recycled waste, offer multiple synergistic advantages, including an enlarged surface area, abundant active sites, improved dispersion stability, and enhanced pollutant adsorption. Critically, their incorporation can reduce the effective bandgap of semiconductors, thereby improving visible-light responsiveness and increasing overall photocatalytic activity [39]. Conventional semiconductors such as TiO_2 and ZnO are well recognized for their environmental compatibility, chemical stability, and low cost. However, their performance remains limited under visible light due to their inherently wide band gaps and rapid electron–hole recombination. Although metal or non-metal doping (e.g., with transition metals or heteroatoms such as N, C, or S) can effectively narrow the bandgap and improve light absorption, excessive dopant concentrations frequently introduce thermal instability, secondary pollution, and even accelerate recombination processes, thereby counteracting the intended enhancements [32, 40]. Accordingly, hybrid

systems that couple doped semiconductors with BMCNS have emerged as a promising strategy to harness the benefits of both components. These hybrids exhibit synergistic effects, combining the electronic modulation from dopants with the adsorptive and conductive properties of BMCNS. However, the fundamental mechanisms by which such hybrid systems enhance photocatalytic activity remain incompletely understood. For example, Yu et al. investigated the electronic structures, optical characteristics, and effective masses of charge carriers in N-, C-, and S-doped ZnO through first-principles density functional theory (DFT) calculations. Their study revealed that due to p-type doping effects, N and C incorporation generated vacant states above the Fermi level and shifted the conduction band toward lower energies, resulting in significant bandgap narrowing and stronger absorption across the visible and UV regions. In contrast, S doping only modestly improved light absorption by directly reducing the bandgap without introducing vacant states. Moreover, effective mass calculations showed that pristine ZnO is intrinsically an n-type semiconductor with light electrons and heavy holes. Doping with N, C, and S generally decreased electron mass and increased hole mass, thereby slowing recombination kinetics. Notably, C doping proved most effective in suppressing electron–hole recombination, offering a particularly promising pathway to enhance the quantum efficiency of ZnO-based photocatalysts [41]. In another example, Hao et al. synthesized a novel phosphorus-doped bismuth oxychloride (P-BiOCl) catalyst and demonstrated its exceptional photo-piezocatalytic degradation of RhB under combined ultrasonic vibration and light illumination. The P–BiOCl exhibited a remarkably high reaction kinetic constant (0.3961 min^{-1}), excellent degradation efficiency (94.7% within 8 min), and outstanding stability compared to pure BiOCl and other reference systems. Both experimental and DFT results indicated that phosphorus doping effectively reduced the bandgap, modulated electronic structure and charge redistribution, and created new electron pathways that promoted charge transfer while suppressing recombination. Additionally, P doping improved the adsorption of oxygen and water molecules, boosting the production of reactive oxygen species ($^{\bullet}O_2^-$ and $^{\bullet}OH$) and substantially enhancing catalytic activity for organic pollutant degradation [42]. Integrating BMCNS into doped semiconductor systems significantly amplifies photocatalytic performance by combining adsorption-driven preconcentration of pollutants with accelerated charge dynamics. The inherently conductive networks and high surface areas of BMCNS enable rapid electron transport, stabilize photogenerated charge carriers, and facilitate effective removal of diverse contaminants, particularly in complex wastewater matrices where single-function photocatalysts often fail.

However, a critical bottleneck for many inorganic nanomaterials lies in their susceptibility to photocorrosion, which not only compromises activity but also generates secondary pollution through ionic leaching. For example, CdS QDs readily undergo photocorrosion under prolonged illumination, as photogenerated holes attack the CdS lattice, leading to structural breakdown into toxic Cd^{2+} and S^- ions. Analogous instability issues have been documented for ZnO and CuO, underscoring the urgency of addressing long-term durability and reusability in photocatalytic systems. While certain metal oxide/BMCNS composites—such as BWO/4%C—have demonstrated improved operational stability [34], the broader literature lacks a systematic evaluation of long-term photostability and photocorrosion in metal-containing BMCNS hybrids. In particular, repeated irradiation cycles can promote gradual oxidative dissolution or migration of embedded metals, and the fate of leached ions such as Cd^{2+}, Ag^+, or Cu^{2+} remains insufficiently understood. This gap is critical because such leaching could lead to secondary environmental contamination, undermine catalyst reusability, and impede scalability for real-world water treatment. Without such stabilization strategies, scaling toward pilot- or industrial-level deployment remains infeasible due to both environmental risks and rapid performance decay. Recent advances highlight that hybrid systems integrating photocatalytic oxidation with the adsorption capacity of BMCNS offer a resilient solution. These synergistic platforms not only enhance degradation efficiency but also buffer against fluctuating water chemistries and operational stresses. A notable example is provided by Shivaji et al., who synthesized green-CdS QDs (G-CdS QDs) with biofunctional polyphenol/chlorophyll shells using an inexpensive tea leaf extract. The hybridized G-CdS QDs exhibited superior photocatalytic activity for methylene blue degradation and, crucially, demonstrated enhanced resistance to photocorrosion compared to conventionally synthesized CdS QDs. The protective organic shell suppressed charge carrier recombination, expanded visible-light harvesting, and most importantly, minimized Cd^{2+} leaching. X-ray photoelectron spectroscopy (XPS) analysis confirmed strong sulfur–polyphenol/chlorophyll interactions as the mechanistic basis for corrosion resistance. Furthermore, biocompatibility assays using zebrafish embryos revealed minimal toxicity, even at elevated concentrations, thereby validating the eco-safety of this green synthesis route [43]. These observations suggest that rational surface engineering—whether through biofunctional coatings, carbonaceous shells, or defect-modulating strategies—will be essential not only for preventing performance decay but also for ensuring that metal-containing BMCNS hybrids do not introduce additional ecological risks during prolonged operation.

These insights emphasize that BMCNS-based hybrid photocatalysts transcend the role of passive supports. Through their tunable surface chemistry, environmental safety, cost-effectiveness, and visible-light responsiveness, they function as active participants in photocatalytic systems—enhancing surface reactivity, mediating charge separation, and enabling synergistic stabilization. Taken together, these multifunctional attributes establish BMCNS hybrids as promising next-generation platforms for sustainable environmental remediation and water purification. Building on this perspective, the next section elaborates on the versatile roles of biomass-derived CNS materials in driving photocatalytic degradation processes.

2.1 | CNSs as Support Structures: Synergize Morphology and Charge Transfer

The photocatalytic performance of semiconductors is intrinsically governed by structural parameters such as particle size and surface area, which directly influence light absorption efficiency and interfacial charge-transfer dynamics. However, semiconductor nanoparticles often experience severe aggregation due to their high surface energy, resulting in reduced active interfaces and weaker pollutant interactions [44]. CNSs, derived

from renewable biomass precursors, offer a high-surface-area and structurally robust support that mitigates this aggregation while providing an ideal platform for controlled nucleation and uniform dispersion of semiconductor nanoparticles. Their surface chemistry, typically enriched with oxygen-containing functional groups, imparts negative surface charges that electrostatically attract metallic cations. This interaction regulates nanoparticle nucleation and growth, ensuring uniform deposition, enhanced interfacial contact, and efficient electron transport pathways, which collectively lead to the formation of abundant catalytically active sites. Zhang et al. demonstrated this concept by synthesizing adsorption–photocatalysis composites composed of Cu_2O/Ag nanoparticles anchored on renewable wood-derived biochar (MBC). The adsorption of CR and MO by MBC@Cu_2O/Ag-3 followed a pseudo-second-order kinetic model, achieving sorption capacities of 264.55 and 178.63 mg g^{-1}, respectively, through the combined effects of electrostatic attraction, hydrogen bonding, and complexation effects. The synergistic interplay between MBC, Cu_2O, and Ag significantly enhanced visible-light absorption, thereby promoting efficient electron–hole separation and charge migration. As a result, photocatalytic degradation efficiencies for CR and MO under visible light reached 98.4% and 97.8%, respectively. Free radical quenching and electron spin resonance (ESR) analyses confirmed that superoxide ($^{\bullet}O_2^-$) and hydroxyl ($^{\bullet}OH$) radicals were the dominant reactive species driving pollutant degradation. This study highlights the potential of biomass-derived carbon materials as multifunctional supports for semiconductor–metal composites, demonstrating their capability to couple high adsorption capacity with superior photocatalytic activity. Such bio-based composite systems not only address water contamination challenges but also align with sustainable development goals through the valorization of renewable natural resources [45].

2.2 | CNS-Semiconductor Composites Enhance Charge Separation and Light Absorption

Beyond their role as physical scaffolds, CNSs significantly improve photocatalytic activity by modulating the electronic structure and charge carrier dynamics of semiconductor composites. Their high electrical conductivity, combined with the presence of heteroatoms (e.g., N, O, S) originating from biomass precursors, facilitates efficient charge separation and suppresses the recombination of photogenerated electron-hole pairs. Alghamdi et al. developed a TiO_2-based photocatalyst anchored on activated carbon derived from pistachio shells (AC-TiO_2), targeting the degradation of complex organic contaminants such as the azo dye Reactive Red 120 (RR 120) and the pharmaceutical ofloxacin (OFL) under UV-A irradiation [46]. The AC-TiO_2 composite outperformed bare TiO_2 in degrading both pollutants due to altered bandgap characteristics and enhanced interfacial charge transport. The proportion of AC loading was found to be a critical determinant of the bandgap and, hence, the degradation kinetics. The presence of heteroatom-enriched AC not only broadened the light absorption spectrum but also contributed to improved charge carrier mobility and reduced recombination rates. The durability of the composite was validated through multiple photodegradation cycles, maintaining consistent performance, while GC-MS analysis identified intermediate products and proposed plausible degradation pathways. These findings underline the composite's potential as a sustainable, cost-effective, and versatile photocatalyst for water remediation applications.

2.3 | CNSs Enhance Adsorption and Catalytically Active Interfaces in Photodegradation Systems

CNSs such as graphene, carbon nanotubes (CNTs), and carbon quantum dots (CQDs) play a pivotal role in photocatalytic degradation systems by enhancing adsorption capacity and introducing surface-active regions. Photocatalytic reactions typically occur across three distinct surfaces: the semiconductor surface, the interface between CNSs and semiconductors, and the surface of CNSs themselves. Due to their inherently high specific surface area (SSA) and the presence of abundant oxygen- and nitrogen-containing functional groups, CNSs act as efficient OP adsorption agents and active carriers for electron transfer in nanocomposite photocatalysts [47]. Graphene, CNTs, and CQDs offer structural benefits such as π-conjugated frameworks, defect-rich edges, and tunable electronic states, all of which facilitate pollutant enrichment at the catalyst surface and provide accessible sites for redox reactions. These carbonaceous matrices can bridge semiconductors and act as conductive scaffolds that enable spatial charge separation, thereby reducing charge recombination and amplifying photocatalytic activity. A representative study by Luo et al. exemplifies this concept through the synthesis of a nitrogen-doped, CoO-decorated carbon catalyst (CoO-N/BC) derived from cotton stalk biomass via impregnation followed by carbonization. The incorporation of CoO nanoparticles and nitrogen functionalities onto the biochar significantly increased the SSA (466.631 versus 286.684 m^2 g^{-1} for pristine biochar), correlating directly with enhanced catalytic performance for peroxymonosulfate (PMS) activation and ciprofloxacin (CIP) degradation. The improved performance was primarily attributed to the well-organized sp^2 carbon network, which facilitated directional electron flow, elevated conductivity, and promoted electron-hole separation. Mechanistic investigations using radical quenching and EPR spectroscopy revealed a synergistic interplay between radical (e.g., $SO_4^{\bullet-}$, $^{\bullet}OH$) and non-radical (e.g., singlet oxygen, $^1O_2$) pathways, with the $^1O_2$-mediated route playing a predominant role. Additionally, carbon-bridge mediated electron transfer—validated by time-resolved CIP dosing experiments—accelerated the degradation process, indicating that CNSs can serve as electron conduits in non-radical oxidation systems. Nitrogen-doped sites, CoO nanoparticles, and structural defects within the carbon matrix were identified as the primary catalytic centers for PMS activation. Electrochemical analyses, including electrochemical impedance spectroscopy (EIS) and linear sweep voltammetry (LSV), further confirmed efficient charge transfer processes, consolidating the hypothesis of a CNS-enabled non-radical catalytic mechanism. This study not only demonstrates a promising route for the valorization of lignocellulosic biomass into functional carbon catalysts but also elucidates the nuanced role of CNSs in steering both radical and non-radical degradation mechanisms for environmental remediation [48].

3 | Sources and Types of Biomass-Derived Carbon Nanostructures

Natural biomass has gained considerable attention as a sustainable, carbon-rich precursor for producing carbon-based nanomaterials, owing to its abundance, low cost, environmental friendliness, unique nanoporous structures, diverse morphologies, and mechanical stability. The microstructural characteristics and elemental composition of the resulting carbon materials are strongly determined by the type of biomass used, making precursor selection critical for optimizing yield and structural properties.

In environmental remediation, carbon materials with high surface area, stability, recyclability, and efficient charge carrier transport are in high demand. Achieving high aromatic carbon content and maximizing carbon yield during thermal carbonization largely depends on precursor quality. For instance, a high oxygen content in the biomass can increase defect density and reduce crystallinity, hindering aromatic carbon formation. Similarly, excessive non-crosslinked or aliphatic compounds release volatile species that inhibit fusion processes, lowering carbon yield. Therefore, ideal biomass precursors should possess high carbon content, a large fraction of highly crosslinked molecules with nanoporous structures, and substantial nitrogen content to enable in situ nitrogen doping for enhanced conductivity [49]. Biomass precursors are broadly classified into plant- and animal-based sources. Plant biomass, produced via photosynthesis, primarily contains cellulose, hemicellulose, and lignin, whereas animal biomass—derived from animal waste or residues—consists mainly of proteins, minerals, and polysaccharides such as chitosan and chitin [18]. Figure 3 illustrates these two main biomass categories, discussed in the following sections.

3.1 | Animal-Derived Precursors

Animal biomass generally exhibits greater compositional complexity owing to the diverse macromolecular constituents such as proteins, polysaccharides, lipids, and mineralized components. This complexity offers unique opportunities for developing BMCNSs with tailored heteroatom functionalities, but it also presents notable processing challenges due to the heterogeneity and stability of certain biopolymers. In this section, several easily obtainable and widely studied animal biomass precursors for BMC synthesis are discussed, along with key insights into their utilization potential and associated challenges.

Proteins are indispensable macromolecules in all living organisms, constituting a major fraction of cellular and tissue structures. Composed of amino acids linked via dehydration–condensation reactions, proteins typically contain ~16% nitrogen by weight. Global meat production exceeds 300 million tons annually, generating vast amounts of protein-rich byproducts. While carbohydrates are readily converted into biofuels such as short-chain alcohols and biodiesel, proteins are less attractive for this route due to the energy-intensive deamination process of protein hydrolysates. Consequently, much of this nitrogen-rich waste remains underutilized. The inherent nitrogen content in proteins offers a direct pathway to in situ synthesis of N-doped carbon materials, which have shown improved catalytic activity, conductivity, and wettability compared to

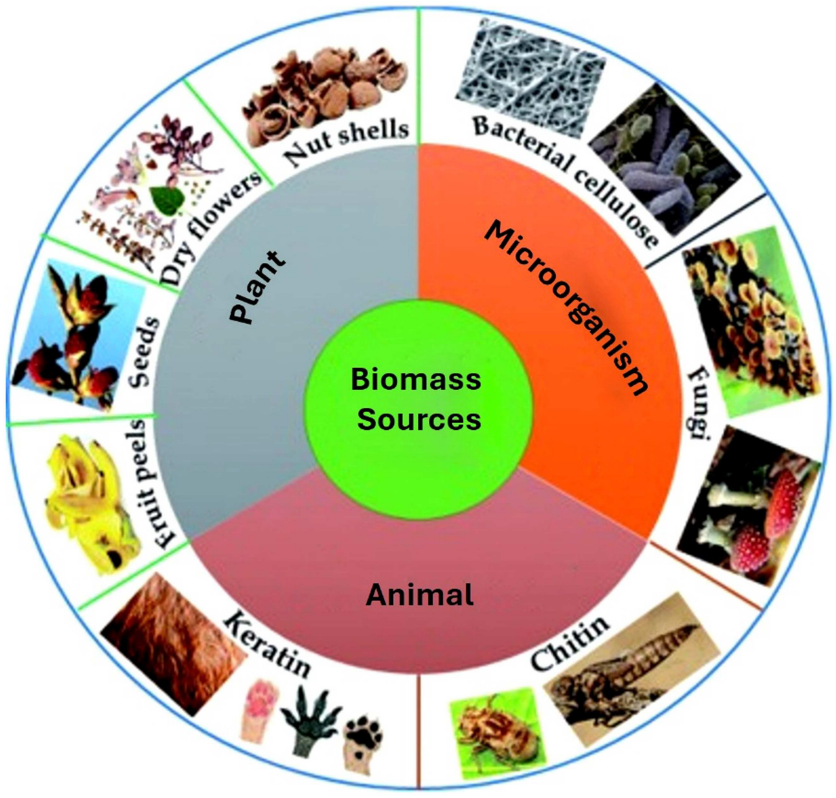

FIGURE 3 | Illustration of major biomass sources. Reproduced with permission from Reference [49], Copyright 2021, RSC.

undoped carbons. However, efficiently retaining nitrogen functionalities during carbonization is difficult, as volatile nitrogen species can be lost at elevated temperatures. Various protein-rich biomasses—milk, silk fibroin, eggs, soybeans, and collagen—have been employed to produce functional carbons. Keratin, abundant in hair and nails, is a notable example. Sinha et al. demonstrated that a controlled carbonization process (holding at 220°C for 1.5 h) suppressed nitrogen volatilization, promoted heteroatom crosslinking, and improved porosity—an approach mirrored in activation steps to further reduce heteroatom loss [50].

Chitin, the second most abundant natural polymer, is a linear polysaccharide composed of β-1,4-linked *N*-acetylglucosamine units with molecular weights reaching up to 1 million. Extensive hydrogen bonding imparts water and alkali insolubility, making extraction and processing challenging. Abundant in crustacean shells and fungal cell walls, chitin accounts for up to 36.43% of shrimp shell mass, positioning seafood waste as a valuable but underutilized source. Its intrinsic nitrogen and oxygen functionalities, together with a hierarchical fibrous architecture, make chitin an attractive precursor for heteroatom-doped porous carbons and carbon–metal–organic framework (MOF) composites. The nanofiber scaffold, with its high aspect ratio (> 100), strong fiber entanglement, and pronounced interaction with water molecules, yields a viscous aqueous dispersion that enhances nanoparticle distribution and prevents sedimentation or aggregation. This property is particularly advantageous for embedding nanosized substances and facilitating uniform metallic deposition. For instance, Choy et al. demonstrated that combining chitin nanofibers with atomic layer deposition enabled the formation of an anatase TiO_2 thin layer across a three-dimensional surface. The resulting composite not only supports TiO_2 nanoparticles through multiple photocatalytic cycles but also achieves notable degradation of gaseous (acetaldehyde) and aqueous pollutants (4-chlorophenol, RhB). Even after repeated reactions, the chitin/TiO_2 system remains intact, with no aggregation or loss of TiO_2, due to the robustness and chemical resistance of the chitin carrier. This stability underscores the potential of chitin-based photocatalysts for treating diverse pollutants under both aqueous and gaseous conditions [51].

Chitosan, obtained from chitin through deacetylation, is the only naturally occurring alkaline polysaccharide. Its abundance of free amino groups not only confers strong metal-ion affinity but also offers multiple reactive sites for structural modification. Soluble in dilute acids, chitosan can be readily processed into hydrogels, aerogels, films, and fibers, enabling precise structural tuning before carbonization to create interconnected porous networks and hybrid composites. In addition to its biodegradability, low toxicity, and strong adsorption capacity, the presence of amino and hydroxyl groups increases the number of active sites for pollutant capture, improving the probability of contact between pollutants and catalysts and thereby enhancing degradation efficiency. Despite these advantages, chitosan suffers from low mechanical strength, limited thermal stability, and modest selectivity in its native form. These drawbacks can be addressed through cross-linking or grafting of active functional groups, which improve stability, adsorption selectivity, and pollutant-trapping capability. For instance, Liang et al. synthesized chitosan-based magnetic nickel ferrite composites ($NiFe_2O_4$/CS, designated CS-LDO) via cross-linking, achieving several key improvements: (1) $NiFe_2O_4$ incorporation increased surface area and generated a porous structure, boosting degradation performance; (2) chitosan effectively inhibited Fe particle agglomeration; (3) the composite activated persulfate (PS) efficiently, enabling high removal rates for both cationic (methylene blue) and anionic (xylenol orange) dyes; and (4) magnetic recovery allowed repeated reuse without significant performance loss. Multiple characterization techniques confirmed the composite's structure and performance, and a detailed reaction mechanism for dye degradation was proposed. This low-energy synthesis route offers a scalable platform for AOPs in treating multi-component dye wastewater [52].

Across animal-derived precursors such as proteins, chitin, and chitosan, a persistent challenge is balancing heteroatom preservation with the generation of high surface area and hierarchical porosity. Strategies including controlled pre-carbonization, chemical activation, and hybridization with inorganic nanostructures have proven effective in mitigating nitrogen loss, preventing structural collapse, and stabilizing functional groups—ultimately enabling the production of high-performance, sustainable BMCNSs from animal waste streams.

3.2 | Plant-Derived Precursors

Plant-derived biomass is the most common precursor category for carbon materials, with its chemical composition varying significantly depending on species and plant part. The main constituents—lignin, hemicellulose, and cellulose—occur in distinct proportions as dried coconut coir contains 46.48 wt% lignin, 21.46 wt% cellulose, and 12.36 wt% hemicellulose, whereas dried hemp consists predominantly of cellulose (67 wt%) with only 3.3 wt% lignin. Scots pine biomass, such as branches and stumps, exhibit high hemicellulose fractions of ~32% and ~28%, respectively. Among these components, lignin shows the highest thermal stability, significantly contributing to the final carbon yield and influencing structural properties. Interactions between lignin and cellulose during pyrolysis (e.g., at 550°C) further affect carbon formation. For environmental remediation applications, ideal biomass precursors should possess high lignin content, low cellulose fraction, and favorable nitrogen/oxygen ratios, enabling enhanced conductivity, controlled defect formation, and higher graphitization [49].

Certain biomass sources, such as plant leaves, are rich in saccharides, proteins, and intrinsic oxide- and nitrogen-based functional groups, making them suitable for advanced photocatalyst design. For instance, Cheng et al. fabricated biomass carbon quantum dots (BQ) from ginkgo leaves and integrated them with rose-flower-like carbon nitride (FCN). The resulting 0D–3D BQ–FCN heterojunction improved exciton dissociation, charge transfer, and light absorption, yielding superior RhB degradation compared with pristine CN, thus demonstrating the potential of forestry waste for metal-free, high-efficiency photocatalysts [53]. Similarly, Fatimah et al. synthesized TiO_2/SiO_2 composite photocatalysts using biogenic silica from bamboo leaves and titanium tetraisopropoxide via a sol–gel method. Characterization (FTIR, SEM, UV–vis DRS, gas sorption) revealed that higher TiO_2 content increased specific surface area, pore volume, and particle size, with band gap energy

peaking at 3.21 eV for 40–60 wt% TiO_2. These composites achieved enhanced methylene blue degradation under UV irradiation, with or without H_2O_2, particularly at 40–60 wt% TiO_2, where photocatalytic performance correlated strongly with higher surface area and optimized band gap energy [54].

Dry flowers comprise organic components, including saccharides, glucosides, vitamins, and proteins, making them a valuable biomass source for carbon materials. Tian et al. utilized bottlebrush flower biomass to prepare nitrogen-doped porous carbons (NPCs) via one-pot thermal activation with $NaHCO_3$ and dicyandiamide. The intensified cross-linking among precursors during pyrolysis enhanced pore formation—especially mesopores—resulting in NPCs with a large SSA of up to 2025 m^2/g. These biomass-derived carbons demonstrated high efficiency in adsorbing and catalytically activating peroxymonosulfate (PMS) for degrading aqueous phenol and *p*-hydroxybenzoic acid (HBA) in both single and binary systems. While the porous structure was found to be more critical for adsorption than surface nitrogen content, the roles of reactive species varied between phenol and HBA degradation [55]. Seeds are another typical plant-derived precursor, favored for their hollow, thin-walled tubular morphology, which is ideal for producing active carbons for environmental applications. Wang et al. developed tangerine seed activated carbon (TSAC) from food waste through one-step pyrolysis, applying it to remove carbamate pesticides (CMs) from complex solutions. The influence of carbonization temperature and time on adsorption performance was examined. Characterization techniques, including FTIR, XRD, Raman spectroscopy, SEM, and nitrogen adsorption/desorption, revealed that TSAC exhibited an SSA of 659.62 m^2/g, a total pore volume of 0.6203 cc/g, and a pore diameter of 1.410 nm [56]. Similarly, fruit peels, often discarded or burned, are rich in fiber and saccharides, making them promising precursors for activated carbons. Wang et al. transformed pomelo peel waste into nitrogen-doped biochar via pyrolysis with sodium bicarbonate and melamine, optimizing conditions to enhance catalytic activity for advanced oxidation applications. The optimized biochar (C−N−M 1:3:4) achieved a high SSA of 738 m^2/g and nitrogen content of 13.54 at%, resulting in excellent performance for PMS activation and removal of sulfamethoxazole (SMX) antibiotics, with 95% removal within 30 min. Its high catalytic activity was attributed to abundant defects, carbonyl groups, graphitic and pyrrolic nitrogen species, and large SSA, facilitating a non-radical oxidation pathway involving singlet oxygen ($^1O_2$) and electron transfer. The biochar also demonstrated remarkable stability and reusability, maintaining 80% removal efficiency after four cycles. Phytotoxicity assays confirmed that degradation intermediates exhibited significantly reduced toxicity in the PMS/C−N−M 1:3:4 system [57].

3.3 | Microorganism-Derived Precursors

Microorganism-derived biomass has emerged as a promising carbon-rich precursor for the fabrication of activated carbon materials, owing to its natural abundance of carbohydrates, proteins, fats, and fibers. Among these constituents, carbohydrates—particularly the chitin present in fungal cell walls—play a dominant role in carbon yield, serving as the primary carbon source during thermal carbonization. In contrast, proteins, fats, and fibers tend to decompose rapidly at elevated temperatures, releasing volatile low-molecular-weight compounds and contributing minimally to residual carbon. Within this context, fungi, especially mushrooms, have been recognized as ideal biomass precursors because of their fast growth rate, wide availability, and notably high nitrogen content (3%–10%). The intrinsic nitrogen within fungal biomass makes it especially attractive for producing nitrogen-doped activated carbons, which often display enhanced adsorption and catalytic properties. For example, Chu et al. utilized the residue of Lentinus edodes to synthesize nitrogen-doped mesoporous activated carbon via phosphoric acid activation. Three samples (MR1, MR2, and MR3) were prepared by varying phosphoric acid impregnation ratios (1, 2, and 3 mL/g). Among them, MR1 exhibited the highest adsorption performance toward pharmaceutical contaminants such as acetaminophen (APAP), carbamazepine (CBZ), and metronidazole (MNZ). Detailed analyses of adsorption isotherms, kinetics, and surface functional groups revealed that the interplay of chemical functionalities and pore structures governed the adsorption mechanism. Furthermore, MR1 was benchmarked against other adsorbents, providing strong evidence for the potential of biomass-derived nitrogen-enriched mesoporous carbons in environmental remediation [58]. Complementing this work, Cheng et al. reported the preparation of nitrogen-doped hierarchical porous carbon (EFS-NPC) from edible fungus slag, an agricultural byproduct, through a simple carbonization–activation route. Owing to the biodegradability and natural infiltrability of fungal hyphae, the resulting EFS-NPC exhibited an exceptional specific surface area (3342 m^2/g), a large pore volume (1.84 cm^3/g), and a well-balanced micropore–mesopore distribution. These features endowed EFS-NPC with outstanding adsorption capacity for BPA, reaching 1249 mg/g, with nearly 90% of equilibrium uptake achieved within just 0.5 h. Moreover, EFS-NPC outperformed commercial activated carbons (Norit RO 0.8 and DARCO granular) in removing 2,4-dichlorophenol (2,4-DCP) and MB. Thermodynamic and kinetic analyses further confirmed that BPA adsorption followed a spontaneous, exothermic, monolayer process [59].

Together, these studies underscore the unique potential of fungus-derived biomass as a low-cost, nitrogen-rich precursor for advanced porous carbons. By leveraging their inherent biochemical composition and structural attributes, fungal residues can be transformed into high-performance adsorbents, offering sustainable and efficient solutions for water purification and environmental remediation.

4 | Influence of Biomass Precursors on Carbon Material Characteristics and Performance

The physicochemical characteristics of biomass precursors critically dictate the structural, functional, and reactive attributes of the derived carbon materials. Lignocellulosic biomass—comprising wood, crop residues, and agricultural byproducts—is primarily constituted of cellulose, hemicellulose, and lignin, which collectively yield high carbon content and enable the development of tunable porous architectures upon carbonization. The decomposition of these oxygen-rich organic constituents introduces abundant surface oxygen-containing groups, thereby enhancing adsorption properties and promoting

interfacial charge transfer during photocatalytic processes. Owing to their inherent porous framework and rich surface chemistry, lignocellulosic biomass-derived carbons (e.g., bamboo biochar, sludge biochar, reed biochar, and spent coffee ground biochar) have been extensively employed as efficient adsorbents and catalysts for environmental remediation. However, variations in the structural and compositional characteristics among different plant-based feedstocks result in distinct physicochemical and catalytic behaviors of the produced biochars [60, 61]. In contrast, algal biomass—rich in proteins, polysaccharides, and lipids—contains relatively higher levels of nitrogen and mineral elements, which promote in situ N-doping and defect formation during pyrolysis. This intrinsic biochemical composition enhances the electrical conductivity and active site density of the resulting carbon materials, thus improving their catalytic performance [62]. Meanwhile, municipal solid waste and food waste precursors, characterized by heterogeneous organic composition and varying inorganic impurities, typically yield amorphous carbons with moderate surface areas. Despite these challenges, advances in modern material science have emphasized the transformation of such abundant and low-cost waste resources into high-quality nanocarbons for environmental remediation applications. Their advantageous physicochemical features—such as adjustable porosity, high surface area, superior adsorption capability, cost-effectiveness, renewability, and chemical/thermal stability—make them attractive sustainable alternatives to conventional carbon materials. Moreover, the catalytic and structural performance of these bio-derived carbons can be further enhanced through activation, heteroatom co-doping, or templating strategies, enabling precise control over pore distribution and surface functionality [63].

Importantly, while these biomass sources offer diverse pathways for engineering carbon nanostructures, their intrinsic compositional variability—arising from seasonal changes, geographical origin, plant/algal species, growth conditions, and waste-stream heterogeneity—is not always sufficiently acknowledged. Such variability can significantly alter the carbon yield, pore evolution during pyrolysis, surface functional group distribution, and heteroatom-doping behavior, ultimately leading to fluctuations in photocatalytic efficiency. To ensure reproducibility and practical scalability, standardization and stabilization strategies are essential. Pretreatment methods such as moisture control, de-ashing, homogenization, and size/particle uniformity, along with biochemical profiling (e.g., lignin/cellulose ratio determination), can help mitigate these inconsistencies. Additionally, adopting controlled carbonization protocols, chemical/physical activation, or blending multiple biomass sources can buffer feedstock variations and yield more consistent physicochemical properties. Integrating such standardization frameworks would considerably strengthen the reliability and application readiness of biomass-derived photocatalysts. Overall, a comparative evaluation of lignocellulosic, algal, and waste-derived biomass precursors (Table 2) reveals that their intrinsic biochemical compositions fundamentally govern the resulting carbon's porosity, doping nature, and catalytic efficiency—offering valuable insights for rational precursor selection and material design in photocatalytic applications.

TABLE 2 | Comparative summary of biomass precursors, key compositional features, and impact on derived carbon performance.

Biomass precursor type	Main composition	Typical properties of derived carbon	Advantages	Limitations	Performance influence
Lignocellulosic biomass (wood, rice husk, coconut shell)	Cellulose, hemicellulose, lignin	High carbon yield, hierarchical porosity, O-functional groups	High surface area, structural stability	Requires high-temperature activation	Enhances adsorption and charge separation
Algal biomass (microalgae, spirulina)	Proteins, lipids, polysaccharides, minerals	N-doped carbon, high defect density	Inherent heteroatom doping improves conductivity	Low carbon yield, complex pretreatment	Boosts catalytic activity via active site enrichment
Food/municipal waste	Carbohydrates, fats, and inorganic salts	Amorphous or semi-graphitic carbon	Abundant, low-cost, sustainable	Variable composition, impurities	Suitable for bulk, low-cost catalysts
Animal waste/chitin-rich biomass	Proteins, chitin, minerals	N-/P-doped carbon nanosheets	High heteroatom content	Odor, impurity control	Enhance redox activity and electron mobility

5 | Functionalization of Biomass-Derived Carbon Photocatalysts for Organic Pollutant Degradation

Biomass-derived carbon-based photocatalysts (Table 3) offer a sustainable and highly effective approach for degrading organic pollutants in aqueous environments, thereby addressing the pressing challenge of environmental pollution [1, 49, 64, 65]. By harnessing abundant, renewable, and low-cost resources—including agricultural residues, plant extracts, and naturally occurring biopolymers—these systems embody the principles of a circular economy, converting waste into value-added photocatalytic platforms [66–68]. Processing techniques such as chemical activation, controlled pyrolysis, and heteroatom doping enable the creation of carbon frameworks with high surface areas, tunable porosity, and superior electronic conductivity. These structural and electronic properties are critical for enhancing visible-light absorption, accelerating charge carrier transport, and facilitating efficient redox reactions during photocatalysis [63]. For example, Luo et al. developed a nitrogen-doped, CoO-loaded carbocatalyst (CoO–N/BC) from cotton stalk biomass through a straightforward impregnation–carbonization route. Compared to pristine cotton stalk biochar, CoO–N/BC displayed a markedly higher specific surface area (466.631 vs. 286.684 $m^2\ g^{-1}$) and superior catalytic activity in peroxymonosulfate (PMS) activation for ciprofloxacin (CIP) degradation. Mechanistic investigations revealed that the well-ordered carbon network promoted directional electron flow, boosting electron migration and conductivity. Both radical and non-radical oxidation pathways were active; however, singlet oxygen ($^1O_2$)–mediated non-radical processes dominated. Moreover, a carbon-bridge–mediated non-radical pathway further accelerated degradation, as confirmed through time-staggered CIP addition experiments. Active sites were attributed to nitrogen dopants, CoO nanoparticles, and structural defects within the sp^2-hybridized carbon lattice. This work not only demonstrates a value-added route for lignocellulosic biomass utilization but also provides mechanistic insight into heterogeneous catalysis by transition-metal–modified biomass carbons [48].

Importantly, the photocatalytic performance of biomass-derived carbons can be significantly amplified via strategic integration with semiconductors, metal nanoparticles, or co-dopants. Such hybrid systems exploit synergistic effects—prolonged photogenerated carrier lifetimes, extended visible-light absorption, and enhanced interfacial charge transfer. Metallic co-catalysts or semiconductor heterojunctions can facilitate spatial charge separation, thus suppressing recombination losses and boosting quantum efficiency [78]. Additionally, the effective utilization of the local surface plasmon resonance (LSPR) effects of metal nanoparticles to improve optical absorption capabilities and inject hot electrons into photocatalysts opens new directions for addressing the problem of solar energy utilization efficiency of photocatalysts. Zhang et al. developed an in-situ technique for preparing plasmon Ag nanoparticles (NPs) decorated with a covalent organic framework (COF), named Ag/TpPa-1-COF. The finite-difference time-domain (FDTD) simulation results reveal that the strongest electric field intensity is present when the catalyst is excited at $\lambda = 465$ nm. The plasmonic "hot spots" induced by the interfacial electric field enhancement factor distribution of Ag/TpPa-1 were simulated in detail by adjusting the number, particle size, and gap distance of Ag NPs. The DFT

TABLE 3 | Summary of key BMCNS photocatalysts and their efficiencies in OP degradation.

Photocatalysts	Bio-waste source	Modification Strategy	Target pollutant (s)	Degradation efficiency (%), time	Light source	Reference
Ag/P@BC	Corn straw	Calcination	Rhodamine B	> 93%, 60 min	Visible light	[69]
AC-TiO_2	pistachio-shell	Calcination	Reactive Red 120	95%, 60 min	UV-light	[46]
BM-BCN	Citron fruit peel	Heating and grinding	Indigo carmine dye	98.3%, 60 min	Visible light	[70]
AC@Fe_3O_4	Tribulus terrestris	Calcination and coprecipitation	Methylene blue	94.6%, 10 min	Visible light	[71]
BPC/g-C_3N_4	Eucalyptus bark	Calcination	Oxytetracycline	84%, 10 min	Visible light	[72]
ZnAl-LDO@BC	Poplar biomass	hydrothermal and pyrolysis	Malachite Green	98%, 90 min	Visible light	[73]
BiOBr/BC	Biochar	solvothermal	17α-ethinylestradiol	99.28%, 20 min	Visible light	[74]
RCAGC	Rice husk	Calcination	methyl orange	100%, 9 min	Visible light	[75]
Fe-N-C/PMS	Sawdust	Pyrolysis	Bisphenol A	97%, 60 min	Visible light	[76]
C/g-C_3N_4	Coconut shell husk	Pyrolysis	Malachite green	97%, 10 min	Ultrasonic irradiation	[77]

calculations show that electron transfer from Ag NPs to TpPa-1 occurs at the Ag/TpPa-1 interface, and N sites in Ag/TpPa-1 exhibit low Gibbs free energy (ΔG_{H^*}) for enhanced photocatalytic reaction, providing new insights into the plasmonic "hot spot" region that performs effectively for photocatalytic reactions [79]. For instance, a Z-type heterojunction photocatalyst composed of porous g-C_3N_4 (PCN), nitrogen-doped biochar (N-biochar), and $BiVO_4$ (NCBN) was synthesized via a hydrothermal process. The NCBN exhibited a significantly larger surface area (42.88 $m^2\ g^{-1}$) compared to $BiVO_4$ (4.528 $m^2\ g^{-1}$), with N-biochar functioning as a conductive channel for charge migration and as a structural bridge for Z-type heterojunction formation. This architecture achieved 92.5% norfloxacin (NOR) removal efficiency and retained 70% performance after four catalytic cycles, with superoxide radicals ($^{\bullet}O_2^-$) identified as the primary reactive species [80]. Similarly, Zhong et al. converted green tea biomass into color-tunable carbon dots and hydrothermal carbon, subsequently coupling them with a C_3N_4/BiOBr Z-scheme heterostructure to optimize band alignment and electron transfer. The resulting composite degraded 98.48% of RhB within 15 min when loaded with 20 wt% red-emitting carbon quantum dots, achieving 4.07× the activity of pristine BiOBr. Electron spin resonance analysis confirmed the generation of both hydroxyl ($^{\bullet}OH$) and superoxide ($^{\bullet}O_2^-$) radicals, revealing a multi-pathway degradation mechanism [81]. Although these examples demonstrate enhanced photocatalytic activity, the underlying interfacial mechanisms—especially in multi-component systems such as Z-scheme heterojunctions and plasmonic hybrids—are not always explored in sufficient depth. Recent studies employing advanced spectroscopic and computational methods, including transient absorption spectroscopy and DFT calculations, provide insights into ultrafast charge migration, electron–hole recombination dynamics, and energy-level alignments at interfaces. Such a mechanistic understanding is critical for rationally designing BMCNS-based hybrid photocatalysts with optimized electron transfer pathways and synergistic interactions [82, 83]. The adaptability of biomass feedstocks supports the tailored synthesis of diverse carbon-based photocatalysts, such as carbon dots (CDs) [84], biochar [85], heteroatom-doped carbons [86], and highly porous carbons. Each architecture offers distinct structural, optical, and electronic features suited for targeted photocatalytic functions, including organic pollutant degradation, hydrogen evolution, and CO_2 photoreduction. Moreover, their green, scalable synthesis routes align with sustainable development goals, making them viable, eco-friendly alternatives to conventional inorganic photocatalysts.

As summarized in Figure 4, biomass-derived carbon photocatalysts can be broadly categorized into six types: (i) pristine carbon photocatalysts obtained directly from biomass; (ii) composites combining biomass carbon with other functional materials; (iii) heteroatom-doped carbons with enhanced electronic structures; (iv) biochar-based systems with hierarchical porosity; (v) carbon nitride–based hybrids enriched in nitrogen frameworks; and (vi) multi-component hybrid photocatalysts integrating complementary active phases. The subsequent sections explore the synthesis methodologies, physicochemical properties, and photocatalytic mechanisms of each category in detail.

5.1 | Functionalized Bio-Waste-Derived CNS Photocatalysts for Pollutant Degradation

BMCNSs have gained increasing attention as sustainable and high-performance photocatalysts, owing to their renewable feedstocks, structural adaptability, and eco-benign synthesis strategies. These materials—encompassing CDs, AC, and graphene-like frameworks—exhibit tunable physicochemical properties, high surface area, and abundant functional groups, all of which enhance light harvesting, charge separation, and catalytic site availability, making them ideal for environmental photocatalysis. A representative example is provided by Qurtulen et al. [87], who synthesized CDs via a one-step hydrothermal process from green tea waste, a biomass resource inherently rich in aromatic and heteroatom-containing compounds. The resulting CDs possessed excellent aqueous solubility, strong fluorescence, and remarkable chemical stability across a wide pH range and concentration window. Under visible-light irradiation, they achieved rapid RhB degradation (97.89% within 30 min), with adsorption behavior fitting the Freundlich isotherm ($R^2 = 0.97$) more closely than the Langmuir model ($R^2 = 0.93$), indicating that adsorption occurred on a heterogeneous surface with sites of varying energy and multilayer adsorption capability, rather than on a uniform monolayer surface as assumed in the Langmuir model. The photocatalytic process followed pseudo-first-order kinetics, suggesting efficient surface-mediated reactions. Such performance highlights the strong potential of biomass-derived CDs for OP removal in wastewater treatment. To further enhance photocatalytic efficiency, heteroatom doping—especially nitrogen doping—has been widely employed due to its ability to narrow bandgap energy, boost charge carrier mobility, and create additional active sites. Hong et al. [88] prepared Fe-anchored nitrogen-doped CDs (Fe-NCDs) via a solvothermal route with post-modification in a choline chloride/$FeCl_3$ medium. The Fe-NCDs, enriched with N/O functional moieties, achieved ~97% methyl orange (MO) degradation under UV light, attributed to synergistic interactions between dopants and anchored Fe sites that enhanced charge separation and reactive species generation (Figure 5a–c). Extending this strategy, dual doping of rice-husk-derived CDs with nitrogen and bismuth at optimal loadings (10% N-CDs, 5% Bi-CDs) further boosted MO degradation, driven by defect-site engineering, photoluminescence modulation, and improved electron–hole separation [89].

Beyond zero-dimensional CDs, biomass-derived AC provides a high-surface-area, conductive scaffold for integrating metal oxides and dopants [90, 92–94]. For instance, Montazeri et al. [92] fabricated TiO_2/AC composites from lignin-derived AC through pyrolysis, sonication, and reflux processes, achieving superior RhB degradation under UV light due to AC-facilitated charge separation and TiO_2's strong UV photoactivity. Building on this, Baruah et al. [90] developed a ternary Ni–TiO_2/AC composite from pine-cone-derived AC via pyrolysis, sol–gel synthesis, and hydrothermal treatment, achieving near-complete anthracene removal (~99.9%) within 50 min under visible light (Figure 5d–f). Ni doping reduced TiO_2's bandgap from 3.2 to 2.4 eV, enabling enhanced visible-light absorption and catalytic activity.

The photocatalytic pathways were further validated by identifying key intermediates such as (1E,3Z)-hexa-1,3,5-trien-1-ol,

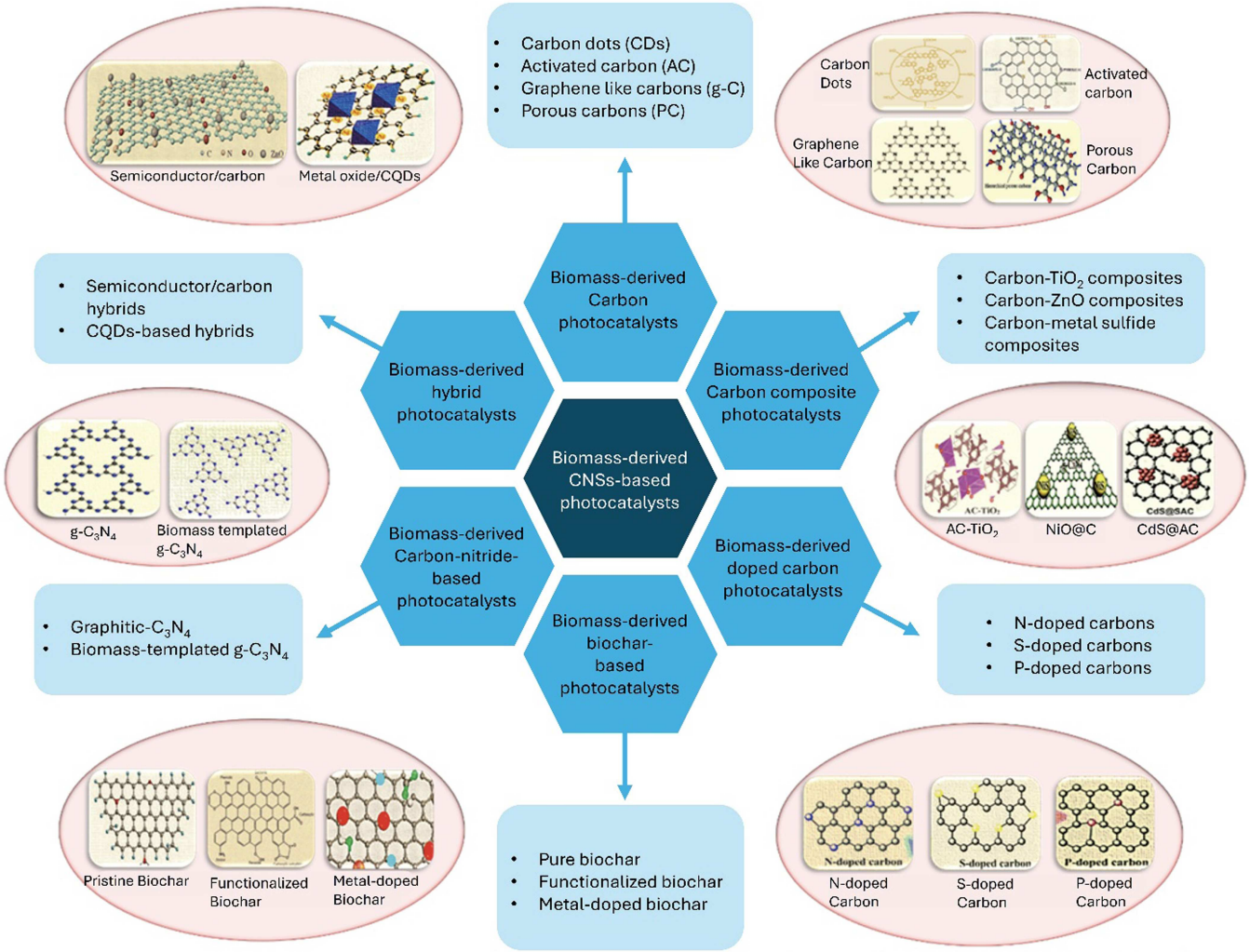

FIGURE 4 | Schematic illustration of biomass-derived carbon-based photocatalysts.

confirming oxidative degradation mechanisms (Figure 5g). This AC-based approach is not limited to TiO_2; incorporation of other metal oxides, such as ZnO, SnO_2, and MnO_2 into AC frameworks has broadened the spectrum of degradable contaminants. For example, Vinayagam et al. [95] produced ZnO/AC hybrids via biomass pyrolysis followed by hydrothermal growth, achieving complete Orange G degradation under both UV and visible light, with excellent recyclability. Similarly, Begum et al. [93] synthesized SnO_2/AC from sugarcane-juice-derived AC, obtaining > 94% Naproxen degradation under sunlight across five reuse cycles. MnO_2/AC composites from peanut shells delivered ultrafast CR removal (~98.5% within 5 min) under dual-light excitation [94], showing how the synergistic interplay between porous AC matrices and redox-active metal oxides can drastically accelerate photocatalytic kinetics.

Beyond traditional transition metal oxides, the strategic incorporation of halogen and noble metal dopants has emerged as a powerful route to modulate the photocatalytic behavior of BMCNSs. For instance, Hu et al. [91] fabricated iodine-doped AC from diverse bio-carbohydrate precursors (rice straw, cow dung), achieving remarkable RhB degradation under visible light. The iodine dopants acted as electron mediators, introducing mid-gap states that prolonged charge carrier lifetimes and facilitated more efficient redox reactions. Similarly, Devi et al. [96] synthesized Ag/AC composites from jute sticks via chemical precipitation, which efficiently degraded malachite green oxalate and clofibric acid under solar irradiation. Here, Ag nanoparticles induced LSPR effects, significantly boosting light harvesting and interfacial charge transfer. Nitrogen doping has also proven highly effective. Dhiman et al. [97] prepared N-doped graphene aerogels (N-GA) through a one-pot pyrolysis of glucose and ammonium chloride, achieving 99.8% telmisartan degradation in 70 min under visible light. The high porosity and abundant N-functional groups enhanced charge mobility and surface reactivity. Extending this approach, Han et al. [98] synthesized Fe–N-doped graphene with a nano-onion-like architecture from Lentinus edodes using $Fe(NO_3)_3$ as the nitrogen source. The abundant edge sites and Fe–N coordination bonds facilitated phenol degradation, while Wu et al. [99] reported a related Fe–N anchored honeycomb carbon (Fe–NC) that degraded tetracycline with 94% efficiency, highlighting the combined importance of hierarchical porosity and catalytically active Fe–N centers. Morphological optimization further amplifies performance. Gupta et al. [100] produced porous carbon from Bengal gram husk (BGBH-C-K) with a graphene-like nanostructure, which showed exceptional dye adsorption, underscoring the role of tailored texture in pollutant removal. Zeng et al. [101] demonstrated that integrating 3D

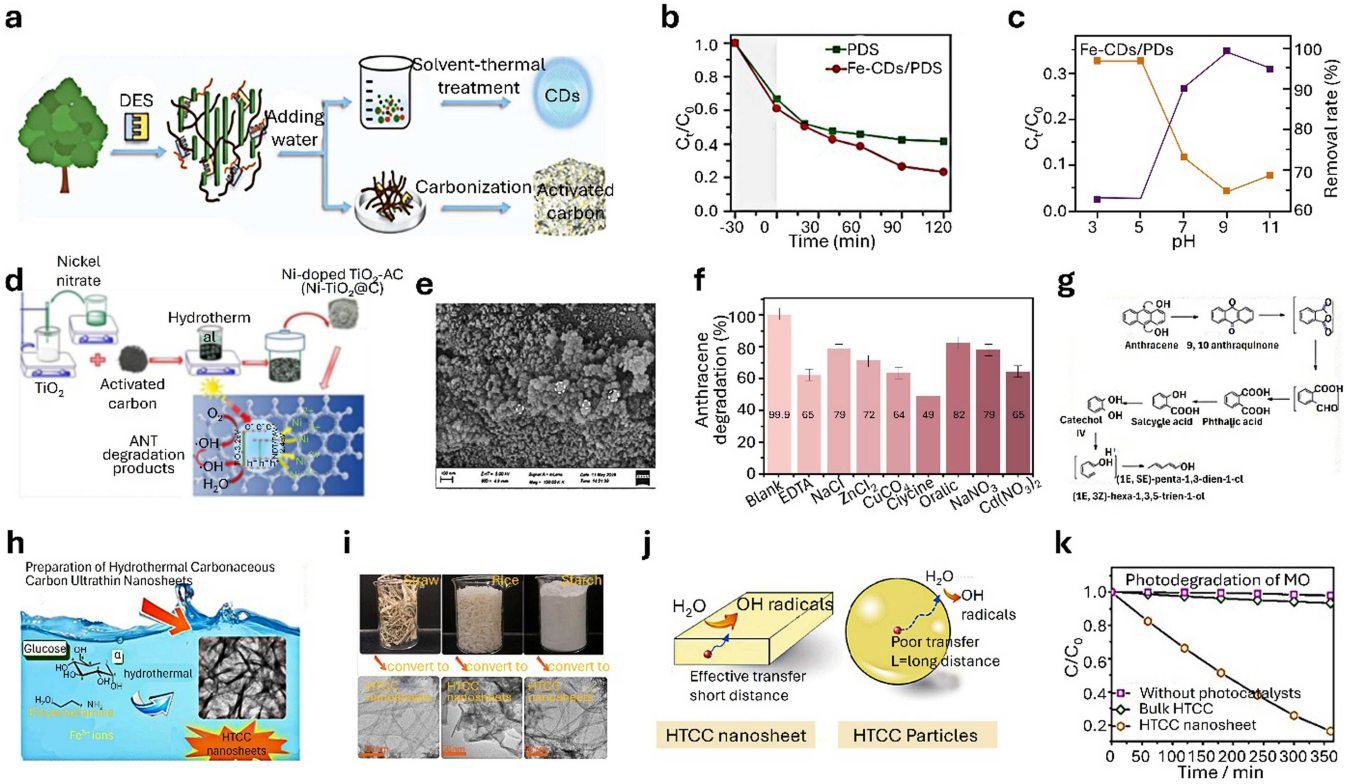

FIGURE 5 | (a) Schematic of eucalyptus fractionation and conversion into CDs and AC, (b) comparison of MO degradation using Fe-CDs/PDS versus pure PDS, and (c) influence of initial pH on MO degradation. Reproduced with permission from Reference [88], Copyright 2024, Elsevier. (d) Illustration of Ni-TiO_2@C nanocomposite and anthracene photodegradation, (e) SEM image of Ni-TiO_2@C, (f) ANT degradation by Ni-TiO_2@C in the presence of interfering ions, and (g) proposed ANT degradation mechanism. Reproduced with permission from Reference [90], Copyright 2022, Elsevier. (h) Schematic of water-based synthesis of HTCC nanosheets, (i) transformation of starch, rice, and straw biomass into HTCC nanosheets, (j) enhanced charge transfer in nanosheet versus bulk HTCC, and (k) MO photodegradation on both forms. Reproduced with permission from Reference [91], Copyright 2022, Elsevier.

graphene with CdZnS nanoparticles—derived from mangosteen peel—enabled 95% ciprofloxacin degradation within just 15 min under solar irradiation, owing to the synergistic combination of high-surface-area conductive scaffolds with visible-light-active semiconductors. Two-dimensional nanosheets obtained via hydrothermal carbonization (HTCC) also exhibit superior charge transfer properties. Hu et al. [91] reported HTCC/Fe_2O_3 composites from starch and rice seed biomass that showed enhanced MO dye degradation under visible light (Figure 5h–k) due to efficient interfacial charge transport and recombination suppression. Beyond metal-based systems, sustainable metal-free photocatalysts have been realized. For example, a C_3S_2/PMS aerogel composite, produced by coupling biomass-derived carbon aerogel with peroxymonosulfate, achieved > 99% oxytetracycline degradation under UV light [102], demonstrating the viability of non-metallic catalytic systems for pharmaceutical pollutant removal. Similarly, Arulasaru et al. [103] synthesized a nanoporous carbon/V_2O_5 composite (NPC/V_2O_5) from hyacinth through hydrothermal treatment and chemical activation, attaining 97.7% berberine hydrochloride degradation within 80 min under visible light, in which V_2O_5 facilitated redox cycling, accelerating the photocatalytic reaction kinetics.

Collectively, these studies reveal that targeted heteroatom doping, noble metal incorporation, and morphological engineering of biomass-derived CNSs consistently yield synergistic enhancements in light absorption, charge separation, and surface reactivity. Such integrative design principles position biomass waste as a sustainable, low-cost, and high-performance feedstock for next-generation photocatalysts aimed at mitigating a broad spectrum of organic pollutants.

5.2 | Functionalized Bio-Waste-Derived CNS Composite Photocatalyst for Pollutant Degradation

An emerging and effective strategy to enhance photocatalytic efficiency is the integration of semiconductors with biomass-derived carbon materials. These carbonaceous supports provide high surface area, excellent electrical conductivity, and abundant reactive sites, which synergistically promote charge separation, extend visible-light absorption, and suppress recombination losses. Among such systems, TiO_2–carbon composites have been extensively investigated due to their strong interfacial interactions and complementary functionalities. The electron-accepting capacity of carbon mitigates charge recombination in TiO_2, thereby enhancing photocatalytic activity. For instance, Pastre et al. [104] developed a 1:1 TiO_2 composite with coconut mesocarp-derived carbon (BCPs400-50:50), achieving efficient MB degradation under visible light. Similarly, Zhang et al. [105] synthesized Clignin-@H-TiO_2 using lignin as a carbon source, which enabled complete atenolol degradation within 5 min under solar irradiation while maintaining activity over 10 cycles, emphasizing durability and

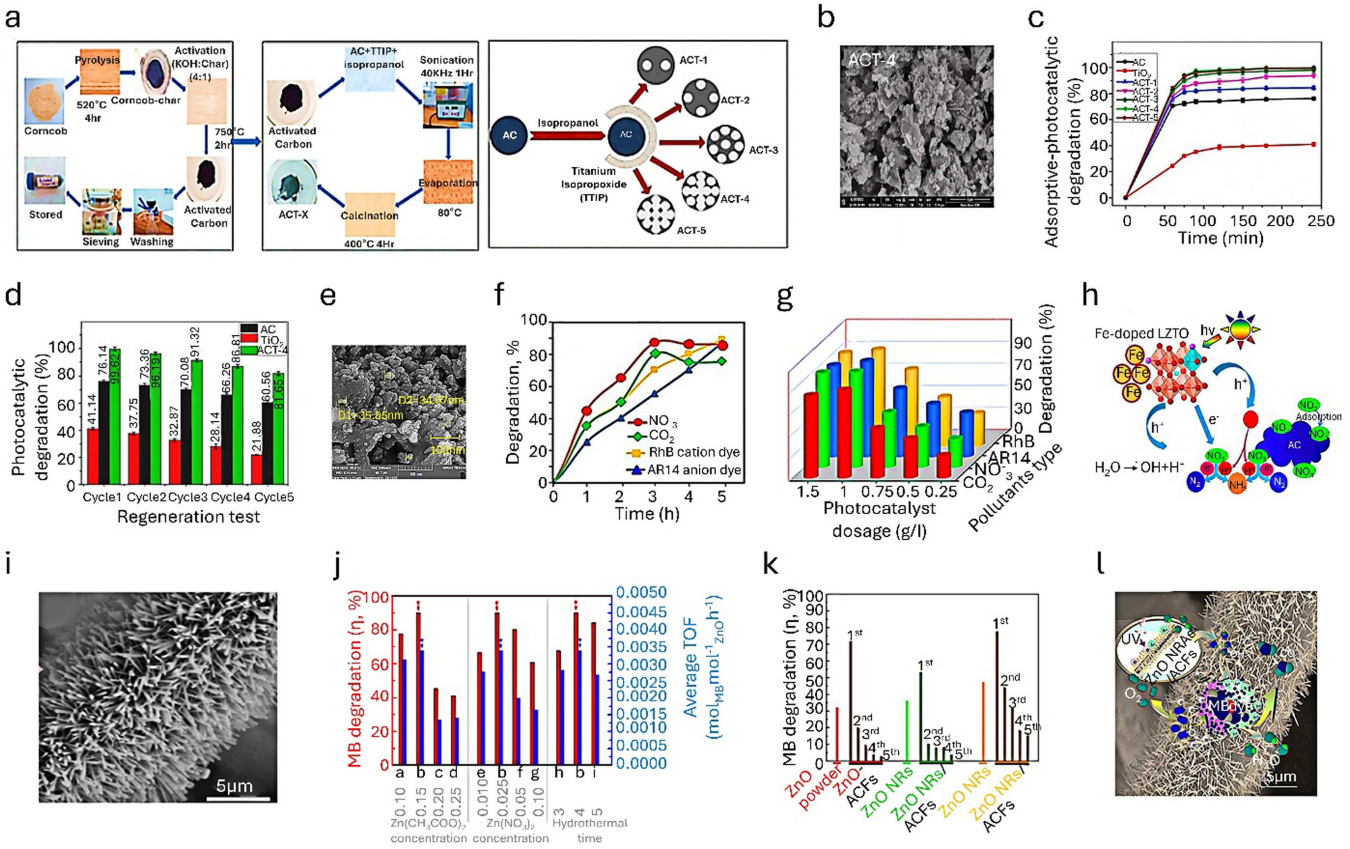

FIGURE 6 | (a) Schematic of the synthesis process for corncob-derived AC, ACT-X composites, and their compositions, (b) SEM image of ACT-4, (c) photodegradation comparison of ceftriaxone (CEF) using TiO_2, AC, and ACT-X photocatalysts, and (d) reusability of TiO_2, AC, and ACT-X. Reproduced with permission from Reference [106], Copyright 2023, Elsevier. (e) SEM image of Fe-doped La_2ZnTiO_6/AC, (f) photocatalytic performance against various pollutants, (g) effect of catalyst dosage, and (h) proposed NO_3^- photodegradation mechanism under visible light. Reproduced with permission from Reference [107], Copyright 2022, Elsevier. (i) SEM image of ZnO NRAs/ACFs, (j) MB dye degradation and average TOF, (k) reusability tests, and (l) proposed MB degradation mechanism. Reproduced with permission from Reference [108], Copyright 2020, Elsevier.

rapid photoresponse. Building on this approach, Abdullah et al. [106] fabricated ACT-X composites from corncob-derived activated carbon and TiO_2 via pyrolysis and sonication. Notably, ACT-4 exhibited 99.6% ceftriaxone degradation under visible light and retained over 80% activity after five cycles. The performance enhancement was attributed to its narrowed bandgap (3.05 eV), improved visible-light harvesting, and efficient generation of ROS such as superoxide and hydroxyl radicals (Figure 6a–d).

The versatility of such composites has been further validated by additional studies. Bukhari et al. [109] employed waste scrap tire-derived AC to fabricate TiO_2–AC nanocomposites via wet chemistry. Increasing AC loading narrowed the optical bandgap by up to 17.17% (direct) and 34.57% (indirect), while creating surface oxygen vacancies that facilitated efficient RhB dye removal (99.14%). This highlights how waste-derived carbons not only serve as sustainable support but also tune the electronic structure of semiconductors. Similarly, Kadkhodayan et al. [107] reported Fe-doped La_2ZnTiO_6/AC composites that degraded multiple pollutants under visible light, with efficiency rising from 20% to 90% as catalyst dosage increased from 0.25 to 1.0 g/L (Figure 6e–h). Ezung et al. [110] advanced this further by developing Fe-doped ZnO/AC nanocomposites, which achieved ~98% chlorpyrifos degradation at a low catalyst loading (0.5%) with excellent recyclability. ACFs have also been recognized as highly effective carbon supports due to their large surface area (1000–3000 m^2/g), strong adsorption capability, and interconnected porous graphitic structure. ACFs enhance visible-light absorption and charge transfer while acting as robust substrates for semiconductor nanostructure growth. For instance, Luo et al. [108] synthesized ZnO nanorod arrays on ACFs (ZnO NRA/ACFs), which showed superior MB degradation under visible light with excellent recyclability. Their enhanced performance was attributed to synergistic interfacial interactions and efficient electron–hole separation (Figure 6i–l). Complementary work by Albiss et al. [111] demonstrated ZnO nanorods grown on ZnO-NP-seeded ACFs via sol–gel and hydrothermal synthesis. The optimized ZnO-NR/ACF composites achieved 99% MB degradation within 2 h, benefiting from enhanced charge transfer, enlarged surface area, and multidirectional light scattering from the flower- and brush-like ZnO morphologies. These composites maintained photocatalytic activity over five reuse cycles, further confirming their stability and practical potential. Beyond fibrous carbons, biomass-derived carbon aerogels (CAs) have emerged as promising supports due to their high porosity, lightweight structure, and eco-friendliness. Shanmugam et al. [112] prepared CA/ZnS–Ag composites via a hydrothermal process, exploiting CA's ability

to prevent nanoparticle aggregation, increase surface area, and improve conductivity. The CA/ZnS–Ag composites achieved 98.64% degradation within 150 min and retained their activity over five cycles. The enhanced performance was attributed to heterojunction formation between CA and Ag nanoparticles, which improved charge separation and visible-light utilization. Collectively, these studies highlight the central role of biomass-derived carbons—whether as activated carbons, fibers, or aerogels—in tailoring photocatalytic properties through structural, optical, and interfacial modifications. By coupling TiO_2, ZnO, or metal sulfides with such carbon supports, photocatalytic activity, stability, and recyclability can be significantly improved. Importantly, the reliance on renewable biomass-derived carbons aligns with green chemistry principles, underscoring their promise for sustainable environmental remediation.

5.3 | Biomass-Derived Doped Carbon Photocatalysts for Pollutant Degradation

Heteroatom-doped carbon-based photocatalysts exhibit enhanced versatility and performance owing to their improved physicochemical characteristics. The incorporation of heteroatoms such as nitrogen, sulfur, and phosphorus into carbon frameworks significantly enhances charge transfer, surface reactivity, and catalytic efficiency. Nitrogen doping is among the most widely investigated modifications. Nitrogen-doped carbon (N-C) [113], often derived from nitrogen-rich biomass such as proteins or chitin, facilitates efficient electron transport, thereby improving photocatalytic performance [114]. Kong et al. [115] synthesized a graphitic carbon nitride–N-doped porous carbon nanocomposite photocatalyst that effectively degraded multiple organic pollutants, including RhB, MB, and TC. Similarly, nitrogen-rich carbon dots (N-CDs) integrated with g-C_3N_4 demonstrated efficient photooxidation of glycerol into ethylene glycol under visible light [116]. Wang et al. [117] further developed a supramolecular imprinted polymer-modified N-doped cellulose film photocatalyst (SMIP@N-CF), which exhibited remarkable efficiency in the detection and degradation of PFOA, attributed to the synergistic generation of reactive oxygen species from nitrogen and carbon dopants. Biomass-derived N-CDs coupled with semiconducting TiO_2 have also been employed for dye removal, where an N-CDs/TiO_2 photocatalyst achieved 62.5% MO dye degradation within 20 min under visible light [118]. Zheng et al. [119] produced N-doped carbon (CN) by delignifying biomass balsa wood powder and further incorporating Fe via ball milling and pyrolysis to form Fe@CN (Figure 7a). The resulting Fe@CN photocatalyst exhibited a honeycomb-like porous structure (Figure 7b,c), effectively decomposing organophosphorus compounds under visible light (Figure 7d) and maintaining high TC degradation efficiency over five reuse cycles (Figure 7e). Similarly, biomass charcoal-supported Ag@C and N-doped TiO_2 defective photocatalysts [120] achieved up to 95% degradation efficiency under visible light, confirming the positive influence of N-doping on photocatalytic performance.

Sulfur doping also enhances photocatalytic reactivity by modulating surface charge and light absorption. Sulfur-doped carbon (S–C) [123], obtained from sulfur-enriched biomass or chemical doping, exhibits faster photocatalytic reaction kinetics. Zhu et al. [124] synthesized sulfur and chlorine co-anchored bio-carbon dots (Bio-CDs) from palm powder, achieving 71.7% and 94.2% degradation of RhB and MB, respectively, under visible light. Lignosulfonate-derived sulfur-anchored carbon (S-C-1-500) also demonstrated effective TC degradation [125], where its photocatalytic properties were governed by reduced band gap energy. Furthermore, Zhang et al. [121] developed cellulose-derived sulfur-doped carbon nanosheets (SCNs) integrated with ZnO via sonication, carbonization, and hydrothermal treatment (Figure 7f). The SCN/ZnO photocatalyst exhibited exceptional photocatalytic performance—achieving over 99% MB degradation (Figure 7g) and efficient degradation of methanol (84%), phenol (92%), and acetone (79%) (Figure 7h). These outcomes were attributed to sulfur and oxygen heteroatoms that enhanced charge separation, transfer efficiency, and visible-light utilization. The strong covalent bonding between ZnO and SCN (C–O–Zn) further imparts stability and recyclability. Dual (N/S) doping strategies have also shown promise; for instance, N, S-co-doped carbon derived from coconut husk effectively detected and removed Ofloxacin contaminants [126].

Phosphorus doping, often derived from phosphate-rich biomass such as bones or shells, tailors the electronic configuration of carbon and enhances photocatalytic activity [122, 127, 128]. Lan et al. [122] fabricated a cornstalk-derived hydrochar–phosphoric acid porous carbon microsphere composite (HC-5P) (Figure 7i), which exhibited superior norfloxacin degradation under visible light compared to other HC–P variants (Figure 7j). The photocatalyst's interaction with different scavengers (Figure 7k) confirmed the role of phosphorus-based functional groups in enhancing adsorption and photodegradation, as illustrated in the proposed mechanism (Figure 7l). Further advancements include olive leaf biomass-derived activated carbon functionalized with polystyrenesulfonate (AC@PSS), achieving 98% MB degradation under UV light [129]. Dual-doped phosphorus and iron-activated carbon (P–F/AC) synthesized from babassu coconut endocarp biomass exhibited synergistic enhancement in MB dye degradation [130]. Likewise, phosphorus-doped carbon coupled with silver phosphate ($AgPO_3$@PC) effectively degraded amoxicillin [127], while self-doped nitrogen and phosphorus porous carbon materials also demonstrated strong photocatalytic activity toward organic pollutants [128]. Collectively, biomass-derived carbon photocatalysts doped with heteroatoms such as nitrogen, sulfur, and phosphorus exhibit superior photocatalytic efficiencies. The introduction of heteroatoms optimizes electrical conductivity, charge carrier separation, and visible-light absorption, thereby accelerating catalytic reactions. Recent developments in dual- and multi-doped carbon structures further highlight their potential as sustainable, high-performance materials for environmental remediation and organic pollutant degradation.

5.4 | Biomass-Derived Biochar-Based Photocatalysts for Pollutant Degradation

Biochar-based photocatalysts have emerged as a promising class of sustainable materials for environmental remediation and solar energy conversion, leveraging their tunable surface chemistry and unique carbonaceous structures. Derived via pyrolysis of biomass, biochar possesses a high surface area, abundant functional groups, and robust structural integrity,

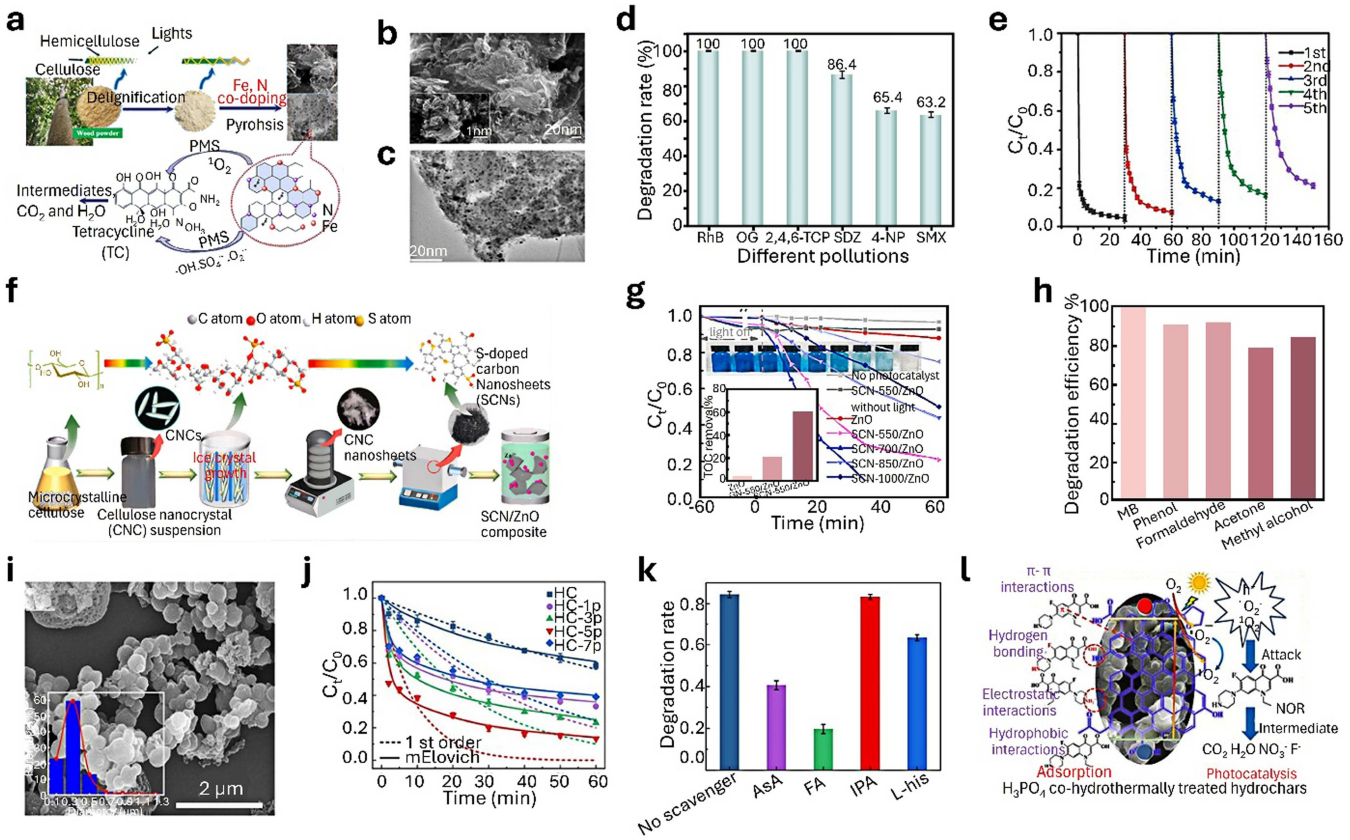

FIGURE 7 | (a) Schematic representation of the fabrication process of Fe@CN photocatalysts, (b, c) SEM and TEM images of as-synthesized Fe@CN photocatalysts, (d) the effect of the presence of co-existing anions as well as humic acid on the photocatalytic degradation performance of Fe@CN photocatalyst, and (e) reusability tests of Fe@CN photocatalyst for the degradation of TC pollutant. Reproduced with permission from Reference [119], Copyright 2023, Elsevier. (f) Schematic illustration of the manufacturing of SCNs and SCN/ZnO composite via carbonization followed by hydrothermal approach, (g) photodegradation performance of MB dye by various photocatalysts (insert: TOC removal of MB solution within 60 min), and (h) photodegradation efficiency of SCN-550/ZnO composite against various OPs under visible light within 60 min duration. Reproduced with permission from Reference [121], Copyright 2022, Elsevier. (i) SEM image of porous carbon microsphere composite (HC-5P) photocatalyst, (j) photocatalytic degradation performance of NOR for HC-5P photocatalyst, (k) the photoreduction of NOR with various scavengers over HC-5P, and (l) schematic showcasing photodegradation mechanism of NO_3^- ion by Fe-doped La_2ZnTiO_6/AC nanocomposite under visible light illumination. Reproduced with permission from Reference [122], Copyright 2024, Elsevier.

which endows it with inherent adsorption capacity and moderate photocatalytic activity [131–133]. While pristine biochar demonstrates baseline photocatalytic behavior through surface-mediated processes, recent advancements have focused on its functionalization and hybridization with co-catalysts to enhance its activity under visible light. One notable strategy involves coupling biochar with transition metal or semiconductor components to improve charge separation and broaden light absorption. For instance, Zheng et al. [134] fabricated a Prussian blue-biomass (PBB) composite using wood-derived biochar, achieving over 95% degradation efficiency of MB dye within 60 min. This synergy between biochar's adsorption capability and Prussian blue's redox activity exemplifies how hybrid materials can amplify photocatalytic response. Similarly, chemical modifications such as metal impregnation (e.g., Cu, Ag, Fe) further enrich the surface reactivity of biochar. These metallic inclusions not only facilitate electron–hole separation but also introduce LSPR effects—particularly in the case of Ag and Cu—enhancing light harvesting and photogenerated charge dynamics. A notable example is the ternary hybrid photocatalyst composed of cotton fiber-derived biochar, Ag-doped g-C_3N_4, and TiO_2, which exhibited superior photocatalytic degradation performance across multiple OPs, including MB, MO, tetracycline (TC), and CR [135]. This multifunctional composite demonstrated how the integration of metal-doped semiconductors with biomass waste-derived carbonaceous scaffolds yields a highly reactive and recyclable photocatalyst. In a separate investigation, Mu et al. [69] developed a novel Ag/P-doped biochar (Ag/P@BC) photocatalyst using corn straw via carbonization followed by a room-temperature solution-stirring process (Figure 8a). The resulting composite displayed a nanoporous architecture embedded with aggregated Ag nanoparticles (Figure 8b), which significantly reduced the bandgap to 2.14 eV. This modification enabled enhanced visible-light absorption and improved charge carrier mobility. Consequently, the Ag/P@BC photocatalyst degraded Rh-B dye 33 times faster than pristine biochar, maintaining over 80% efficiency even after five photocatalytic cycles (Figure 8c,d).

Additionally, metal-oxide-modified biochars are gaining attention for their multifunctional roles. Xin et al. [136] synthesized a $CuFeO_2$-loaded, N/O self-doped biochar composite that

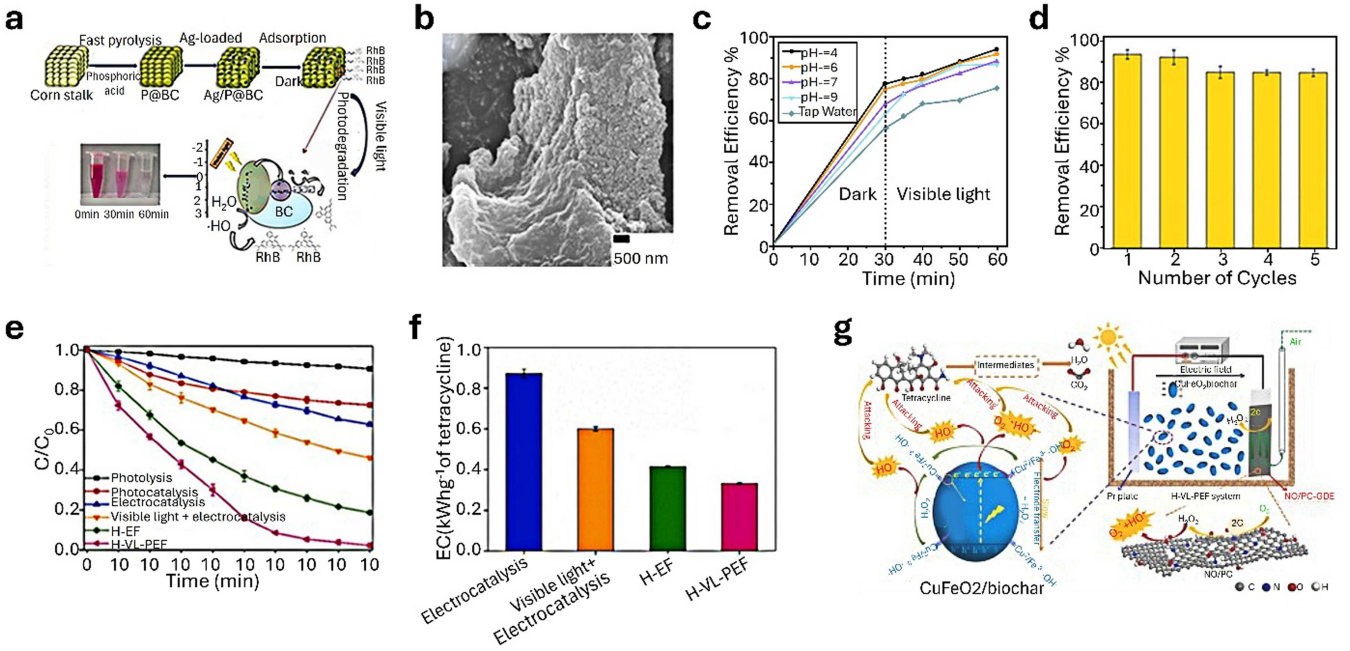

FIGURE 8 | (a) Fabrication schematic and RhB degradation mechanism of Ag/P@BC photocatalysts, (b) SEM images of Ag/P@BC, (c) photocatalytic RhB degradation at different pH levels, and (d) recycling performance of 1Ag/P@BC for RhB removal. Reproduced with permission from Reference [69], Copyright 2021, Elsevier. (e) TC degradation using $CuFeO_2$/Biochar under various systems (visible light + electrocatalysis, H-EF, H-VL-PEF), (f) TOC removal efficiency across systems, and (g) proposed TC degradation pathway in H-VL-PEF. Reproduced with permission from Reference [136], Copyright 2022, Elsevier.

demonstrated efficient tetracycline degradation under visible light in various coupled systems (electrocatalysis, H-EF, and H-VL-PEF), as illustrated in Figure 8e–g. These systems not only enhanced total organic carbon (TOC) removal but also elucidated a stepwise degradation pathway, offering mechanistic insight into the pollutant breakdown process. Similarly, Wang et al. [137] introduced a Fenton-like Fe@BC catalyst derived from sawdust waste, which achieved 92.7% degradation of RhB under visible light within 140 min, highlighting the role of iron in accelerating redox cycles and generating reactive oxygen species. Other doped systems, including NiO [138] and ZnO [139], also demonstrate promising results when integrated with biomass-derived biochar, with hybrid architectures like ZnO/TiO_2/Biochar composites delivering robust degradation of OPs [140–143].

Collectively, these studies underscore the adaptability of biochar as a functional matrix for developing high-performance photocatalysts. By harnessing biomass waste and augmenting its physicochemical properties through metal doping and hybridization with semiconductor materials, researchers have created highly effective photocatalytic systems for environmental purification. These biochar-based composites not only address sustainability by utilizing agricultural residues but also offer scalable solutions for wastewater treatment and solar-driven catalysis. Their ability to operate under visible light, coupled with reusability and structural tunability, marks them as next-generation materials for green environmental technologies.

5.5 | Biomass-Derived Carbon Nitride-Based Photocatalysts for Pollutant Degradation

Graphitic carbon nitride ($g\text{-}C_3N_4$), a promising biomass-derived photocatalyst, has garnered increasing attention due to its tunable electronic structure, visible-light responsiveness, and sustainable synthesis from nitrogen-rich organic precursors such as urea, melamine, and chitosan. The adoption of biomass templates—including natural matrices like leaves, petals, shells, and agricultural residues—introduces hierarchical porosity and surface roughness, which significantly enhance the SSA and increase active site exposure. These features collectively amplify photocatalytic performance, making $g\text{-}C_3N_4$-based materials highly attractive for environmental remediation and solar-to-chemical energy conversion applications. Shakunthala et al. [70] utilized biomass waste in the form of citron peel to develop a $g\text{-}C_3N_4$-based photocatalyst (BM-BCN) for degrading the textile dye indigo carmine. Under natural sunlight, the catalyst achieved an impressive degradation efficiency exceeding 98%, demonstrating the efficacy of bio-templating in enhancing photoreactivity. In a related study, Liu et al. [144] synthesized an N, P co-doped carbon quantum dot/$g\text{-}C_3N_4$ composite (N, P-CQDs/$g\text{-}C_3N_4$) using pulp fiber biomass and melamine as starting materials. The resulting catalyst exhibited superior photocatalytic degradation efficiency (95.5%) toward aromatic pollutants like benzaldehyde, benzoic acid, and phenyl formate, attributable to enhanced charge separation and synergistic light absorption facilitated by the doped CQDs. Expanding the utility of biomass-derived carbonaceous materials, another work [145] demonstrated the successful conversion of glycerol into value-added products using a CQDs/$g\text{-}C_3N_4$ photocatalyst, again sourced from biomass waste. Furthermore, the incorporation of loofah and chitosan into a $g\text{-}C_3N_4$-based hydrogel matrix yielded a flexible and porous photocatalyst capable of degrading a variety of organic pollutants under visible light irradiation [146]. These developments underscore the versatility of biomass scaffolds in tuning $g\text{-}C_3N_4$'s structure-function relationships.

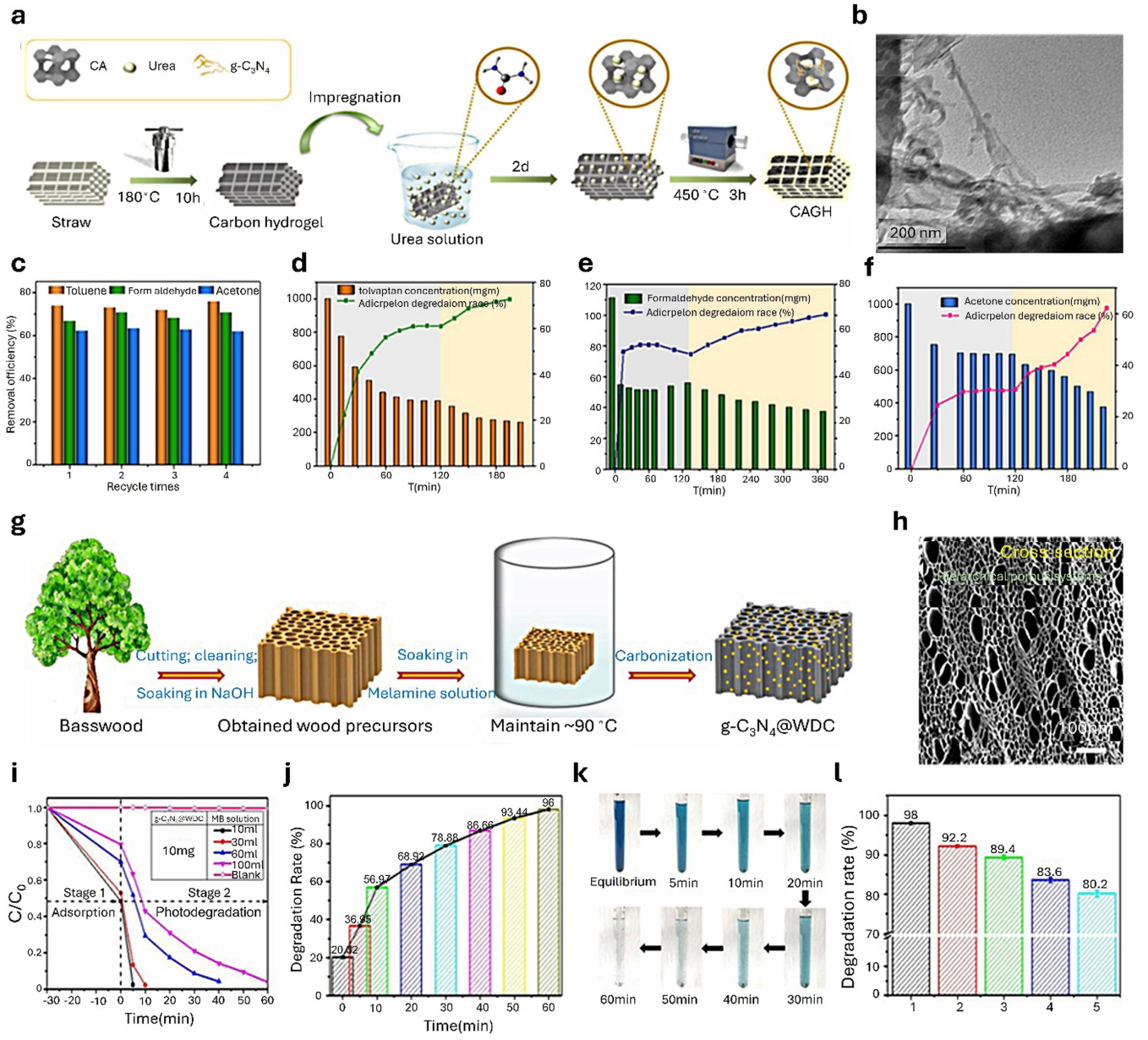

FIGURE 9 | (a) Schematic of CAGH photocatalyst fabrication, (b) TEM image of synthesized CAGH, (c) cyclic photocatalytic degradation test of toluene, formaldehyde, and acetone, (d–f) degradation profiles of these pollutants using CAGH. Reproduced with permission from Reference [147], Copyright 2025, Elsevier. (g) Schematic of g-C_3N_4@WDC synthesis. (h) SEM image of g-C_3N_4@WDC, (i) MB concentration change over time, (j) photocatalytic degradation rate of MB, (k) time-lapse images of MB fading, and (l) recyclability over five cycles. Reproduced with permission from Reference [148], Copyright 2021, Elsevier.

Cheng et al. fabricated a carbon aerogel–g-C_3N_4 hydrogel (CAGH) composite via a hydrothermal synthesis and carbonization route using agricultural straw and urea as precursors [147]. The schematic in Figure 9a outlines the fabrication strategy, while TEM imaging (Figure 9b) confirms the uniform distribution of g-C_3N_4 within the carbon hydrogel network. The resulting photocatalyst exhibited excellent performance in the degradation of VOCs such as toluene, formaldehyde, and acetone (Figure 9c–f), showing not only high activity but also robust recyclability. The hierarchical porous architecture and homogeneous integration of g-C_3N_4 into the aerogel matrix substantially enhanced the number of exposed catalytic sites and improved charge transfer dynamics.

Complementing this, Wu et al. [149] engineered a g-C_3N_4@WDC photocatalyst by loading g-C_3N_4 onto wood-derived porous carbon via carbonization of basswood and melamine (Figure 9g). The SEM image (Figure 9h) reveals a highly porous and interconnected network. The composite demonstrated remarkable photocatalytic degradation of MB dye, achieving 98% degradation within 1 h (Figure 9i–k), and retaining over 80% efficiency after five reuse cycles (Figure 9l). This impressive performance is attributed to the synergistic effect of basswood-derived carbon, which enhances pollutant adsorption, and g-C_3N_4, which accelerates photodegradation under visible light. In addition to pure g-C_3N_4 systems, researchers have explored hybrid composites incorporating metal

and metal oxide species with biomass-derived g-C_3N_4 to further optimize performance. Notable examples include MoO_3/g-C_3N_4 [150], Mn_3O_4/g-C_3N_4 [151], and g-C_3N_4/$FeIn_2S_4$ [152], each showing improved photocatalytic activity through heterojunction formation, improved charge separation, and broader light harvesting. These composite systems benefit from the dual advantages of metal-based redox activity and biomass-templated structural refinement. Overall, the eco-friendly fabrication, structural tunability, and reusability of biomass-derived g-C_3N_4 photocatalysts present a sustainable pathway toward high-efficiency environmental remediation. Recent innovations have demonstrated how integrating waste valorization strategies with advanced nanostructuring techniques can significantly enhance photocatalytic performance. The evolution of such multifunctional systems not only aligns with circular economy principles but also paves the way for next-generation solar-driven degradation technologies.

5.6 | Biomass-Derived Carbon-Based Hybrid Photocatalysts for Pollutant Degradation

Hybrid photocatalysts represent a sustainable and forward-looking approach to enhancing photocatalytic processes, particularly in the realm of environmental remediation. A growing focus has emerged on biomass-derived carbon–semiconductor composites, where renewable carbon sources integrate with semiconductors such as TiO_2, ZnO, and $BiVO_4$. These hybrid systems demonstrate synergistic interactions that improve light absorption, promote efficient charge carrier separation, and enhance overall photocatalytic activity—critical features for the degradation of OPs under visible light. For instance, the integration of activated charcoal (AC) with Bi and TiO_2 (AC-Bi/TiO_2) resulted in a hybrid photocatalyst that effectively degraded MB dye under visible light irradiation [153]. This underscores the cooperative interplay between the high surface area and adsorptive nature of AC and the photocatalytic attributes of Bi and TiO_2. Similarly, AC/$BiVO_4$ composites demonstrated significant potential for OP photodegradation, reinforcing the functional compatibility of biomass-derived carbon and $BiVO_4$ [154]. Extending this strategy, vanadium-doped lignin-derived AC was combined with $BiVO_4$ to create a V-AC/$BiVO_4$ hybrid, which exhibited superior visible-light-driven photocatalytic performance for OP degradation [155]. The doping of V not only narrowed the bandgap but also introduced active sites favorable for redox reactions.

Further expanding this paradigm, Rasouli et al. [156] synthesized a hybrid photocatalyst comprising α-Fe_2O_3, WO_3, and AC derived from Rosa Canina seed debris, which showed excellent photocatalytic degradation efficiency for doxycycline. This work illustrates the benefits of multi-component heterostructures, in which iron and tungsten oxides contribute complementary redox potentials and enhance charge separation, while the biomass-derived AC facilitates pollutant adsorption and dispersion of active species. Other innovative hybrid photocatalysts include combinations of metal/metal oxides and noble metals with biomass waste-derived carbon supports. Notable examples are the CA/ZnS-Ag hybrid composite [112], NiO/PdO@C ternary hybrid structure [157], AC/CeO_2/ZnO [158], and Zinc oxide activated charcoal polyaniline (ZACP) [159]. These systems leverage the plasmonic effects of noble metals, tunable band gaps of metal oxides, and the electronic conductivity and surface functionality of carbon support, resulting in enhanced photogenerated charge transfer and ROS generation.

A compelling illustration of the multifunctional potential of biomass-derived hybrid photocatalysts is provided in Figure 10. Researchers developed a $NiCo_2O_4$–carbon nanocomposite (NCC) synthesized from porous carbon obtained from biomass Bidens using a facile hydrothermal–calcination route [160]. The nanoflower-like NCC structure (Figure 10b), composed of ultrathin $NiCo_2O_4$ nanosheets anchored on carbon, demonstrated excellent photocatalytic degradation of 4-acetamidophenol (AP) across varying concentrations and pH conditions (Figure 10c,d). Furthermore, it exhibited broad-spectrum activity against phenol and aspirin pollutants (Figure 10e), as well as strong recyclability (Figure 10f), indicative of structural and chemical robustness. The plausible degradation mechanism (Figure 10g) highlights the role of synergistic redox cycles between Ni^{2+}/Ni^{3+} and Co^{2+}/Co^{3+}, coupled with the conductive carbon matrix facilitating electron transfer. Similarly, Zhang et al. developed a ternary ZnO/ACSC@TiO_2 hybrid photocatalyst (Figure 10h), utilizing coconut shell-derived carbon (ACSC) as a sustainable support [161]. The material exhibited high photocatalytic degradation efficiency toward RhB and tetracycline (TC) under direct sunlight (Figure 10j–l), maintained catalytic stability across cycles (Figure 10m), and followed an efficient degradation pathway (Figure 10n). The high activity of this system is attributed to (i) a favorable core–shell structure enabling improved OP adsorption and visible light response due to bandgap tuning and (ii) the inclusion of ZnO, which helps suppress charge recombination and contributes to reactive species generation.

Beyond conventional metal oxide systems, hybrids incorporating biomass-derived CQDs have emerged as highly promising photocatalysts owing to their unique quantum confinement effect and up-conversion photoluminescence, which collectively extend visible-light utilization [162]. For instance, TiO_2/CQD composites synthesized using green banana-derived CQDs demonstrated remarkable photocatalytic activity against a range of organic pollutants (MB, RhB, and TC), achieving degradation efficiencies of 89%, 93%, and 94%, respectively, under visible light irradiation [163]. These results highlight the potential of CQD–TiO_2 hybrids as efficient and versatile photocatalysts for wastewater purification targeting dyes, pharmaceuticals, and other emerging contaminants. In a related work, Si et al. engineered biomass-CQDs coupled with BiOCl (CQDs/BiOCl) as a model system to investigate visible-light photodegradation mechanisms. The composite removed 90% of BPA within 2 h under visible light, a performance attributed to C-localized states (CLS) introduced by CQDs that facilitated electron transfer and hole (h^+) generation in the BiOCl valence band. The holes played the dominant role in BPA degradation. Electrochemical analyses and theoretical calculations further confirmed that CQDs enhanced both charge separation efficiency (η_{CS}) and charge injection efficiency (η_{CI}). Moreover, mechanistic studies proposed five possible BPA degradation pathways, supported by ecotoxicity evaluation of intermediates using ECOSAR. While most intermediates showed reduced toxicity for fish, daphnids, and algae, a few (P10 and P12) exhibited exceptions. Overall, this study validated the dual role of biomass-derived CQDs in improving photocatalytic efficiency while simultaneously ensuring ecotoxicity mitigation during

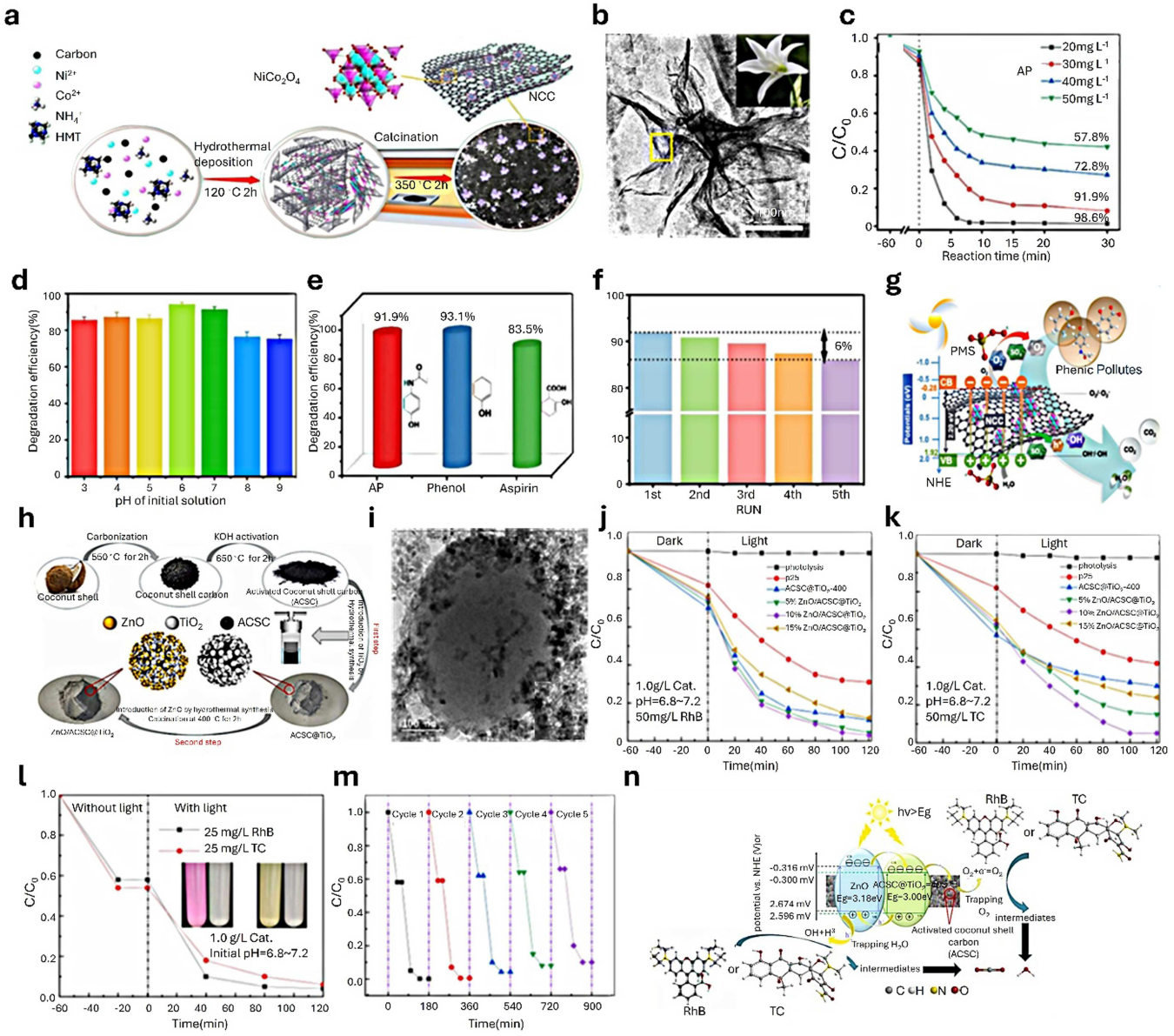

FIGURE 10 | (a) Schematic of NCC photocatalyst fabrication from bidens, (b) HR-TEM image of NCC, (c) pollutant concentration versus degradation performance, (d) degradation efficiency at different pH levels, (e) photodegradation of 4-acetamidophenol (AP), phenol, and aspirin, (f) reusability of NCC, and (g) proposed AP degradation pathway. Reproduced with permission from Reference [160], Copyright 2022, Elsevier. (h) Schematic of ZnO/ACSC@TiO_2 synthesis, (i) TEM image of ZnO/ACSC@TiO_2, (j, k) photodegradation curves of RhB and TC, (l) time-dependent degradation under sunlight, (m) reusability test for RhB, and (n) proposed degradation pathway of RhB and TC. Reproduced with permission from Reference [161], Copyright 2024, Elsevier.

BPA degradation [164]. Complementary evidence of the multifunctionality of biomass-derived carbons was provided by Paghaleh et al., who fabricated a basil-seed-derived r-GO/CuO/$CuFe_2O_4$ heterostructure for oxytetracycline (OTC) degradation. The optimized $CuFe_2O_4$/CuO–graphene-like carbon composite exhibited a degradation efficiency of 87.49% within 90 min and a photoreaction rate constant of 0.0495 min^{-1}. This enhanced performance was linked to superior visible-light absorption, strong interfacial electric fields, suppressed charge recombination, and robust redox capacity arising from an S-scheme heterojunction. Importantly, its high stability and recyclability were verified experimentally and modeled through 3D computational fluid dynamics (CFD) and central composite design (CCD), demonstrating the feasibility of scaling up eco-friendly synthesis routes for practical water treatment applications [165]. A different biomass-derived hybrid approach was presented by Negoescu et al. [166] who introduced dual-metal (Fe and Ti)-doped TiO_2/activated carbon (AC) composites for Congo red photodegradation. The synergistic interplay between Fe–Ti dopants and the porous AC matrix provided enhanced adsorption sites and photodegradation activity, yielding an efficiency of 84.46% under visible light in acidic conditions. Mechanistic studies, aided by scavenger experiments, confirmed the cooperative role of adsorption and photocatalysis in pollutant removal, further linked to the zero-point charge (ZPC) of the nanocomposites.

Taken together, these examples underscore the strategic advantages of biomass-derived carbon-based hybrids: (i) the availability of low-cost and sustainable precursors, (ii) enhanced light harvesting due to tunable electronic structures, (iii) improved pollutant adsorption enabled by porous carbon morphologies, and (iv) efficient charge transfer across heterogeneous interfaces. Nonetheless, reproducibility and performance consistency remain constrained by the inherent variability of biomass feedstocks. Overcoming these challenges will require standardized treatments of carbon precursors, precise heteroatom doping strategies, and advanced interface engineering (e.g., plasmonic coupling and heterojunction formation) to optimize solar-driven photocatalysis. More critically, the field must shift toward systematic investigations of two unresolved issues: (a) quantitative optimization of the adsorption–catalysis synergy via targeted surface functionalization and (b) elucidation of pollutant–catalyst interfacial interactions in realistic, complex water matrices. Addressing these challenges will be key for transitioning biomass-derived hybrid photocatalysts from exploratory demonstrations to rationally designed systems for scalable environmental remediation.

5.6.1 | *Quantitative Optimization of the Adsorption–Catalysis Synergy via Functionalization Control*

A key challenge in the field remains the quantitative understanding and optimization of the synergistic relationship between adsorption and photocatalysis, both of which are essential for effective pollutant degradation. Biomass-derived carbon materials naturally offer abundant surface functional groups (e.g., –OH, –COOH, $–NH_2$), tunable porosity, and defect-rich structures that collectively enhance their ability to adsorb pollutants and facilitate photochemical reactions. However, the specific role of each functional group or heteroatom dopant (e.g., N, S, P, B) in mediating these dual functionalities remains unclear.

Recent advances have highlighted the importance of modulating localized electronic states in carbon nanomaterials to advance adsorption and photocatalytic properties simultaneously. For instance, Duan et al. demonstrated that N-doped graphitic biochar, containing electronegative quaternary nitrogen, induced asymmetric spin density and reduced electron density, which jointly promoted both the adsorption and oxidative degradation of organic pollutants [167]. Similarly, Yang et al. achieved enhanced charge separation and surface catalytic activity by introducing electron spin polarization into carbon nitride sheets through in situ Se doping [168]. Notably, the adsorption behavior of pollutants on carbon surfaces critically dictates the subsequent photocatalytic degradation kinetics via two interrelated pathways. First, adsorptive enrichment near active sites generates a pronounced "local concentration effect," where reactant molecules accumulate within nanometer-scale domains around photoactive centers. This localized enrichment enhances the probability of interfacial redox reactions, thereby increasing the apparent rate constant of photocatalytic degradation. Second, strong interfacial interactions—such as π–π stacking, hydrogen bonding, or electrostatic attraction—establish electron transfer bridges between the adsorbed pollutants and the carbon matrix. These bridges enable charge shuttling, allowing photogenerated electrons to migrate efficiently toward molecular oxygen or other acceptors while minimizing recombination losses. Such effects are particularly enhanced in heteroatom-doped carbon frameworks, where dopant-induced defects act as electron traps and promote charge delocalization across the pollutant–catalyst interface [169]. Building on this, Zhu et al. synthesized pristine covalent triazine frameworks (CTF-1) and systematically incorporated P, S, and Se heteroatoms via high-temperature annealing to examine their influence on dual-functionality. Using benzophenone (BP), 4,4′-dihydroxybenzophenone (DHBP), and 2,2′,4,4′-tetrahydroxybenzophenone (BP-2) as model pollutants, they demonstrated that electron accumulation at nitrogen sites adjacent to heteroatoms directly influenced adsorption energy, while dopant-induced spin polarization substantially enhanced photocatalytic activity [170]. Similarly, Cheng et al. designed a biochar-supported $2Zn_3In_2S_6/WO_3$ (BC/2ZIS/WO_3) photocatalyst via a hydrothermal route, achieving a synergistic balance between adsorption and photocatalysis. The biochar carrier, featuring a large surface area (1161.25 m^2/g) and high electrical conductivity, facilitated charge separation and boosted overall catalytic performance. Adsorption isotherm studies revealed maximum adsorption capacities of 120.04 mg/g for MB and 466.55 mg/g for RhB, while under combined adsorption–photocatalysis, the corresponding removal efficiencies reached 80.5% and 99%, far exceeding those of the bare heterojunction. Complementary DFT calculations, trapping experiments, and HPLC–MS analyses further elucidated the adsorption–degradation mechanisms and pathways, highlighting the critical role of biochar in optimizing interfacial charge transfer and pollutant decomposition [171]. Overall, the strong correlation between adsorption energy and charge transfer dynamics underscores that efficient adsorption not only concentrates pollutants but also aligns their electronic energy levels with the catalyst's conduction or valence bands, thereby enhancing orbital overlap and accelerating interfacial electron exchange.

5.6.2 | *Mechanistic Understanding of Pollutant–Catalyst Interactions in Complex Water Matrices*

Most laboratory studies are conducted under idealized conditions (e.g., single pollutant, neutral pH, DI water), which do not represent the complexity of real wastewater. In practical scenarios, multiple coexisting pollutants (e.g., pharmaceuticals, dyes, heavy metals), variable pH, ionic strength, and natural organic matter can significantly alter the surface chemistry, photocatalytic pathways, and product selectivity. Under such complex matrices, competitive adsorption and co-adsorption phenomena can modulate local concentration gradients and perturb electron-transfer equilibria, thereby dynamically reshaping the adsorption–photocatalysis synergy. Real-time tracking of intermediates using in situ spectroscopies revealed that pollutant–catalyst interactions are highly dynamic and condition-dependent. Therefore, it is essential to explore how pollutants of differing polarity, molecular size, and functional groups interact with specific catalyst sites under complex environmental matrices. Advanced tools such as DFT simulations, reactive molecular dynamics, and in situ FTIR, Raman, and XPS can help unravel the molecular-level adsorption geometries, charge transfer processes, and degradation pathways [172, 173].

6 | Challenges and Prospects of Biomass-Derived CNS Materials

BMCNS have emerged as a promising class of materials for the photocatalytic degradation of OPs, owing to their inherent sustainability, cost-effectiveness, and multifunctionality. These materials exhibit a synergistic blend of adsorption and photocatalytic capabilities, which facilitates efficient decomposition of pollutants. However, translating laboratory-scale success into real-world water treatment applications remains challenging due to several technical, economic, and environmental constraints. A significant barrier to the large-scale adoption of CNS materials is their complexity of production and cost efficiency. While biomass offers an abundant, renewable carbon source, transforming these precursors into high-performance CNS often requires energy-intensive pyrolysis, activation, or doping processes. Compared to conventional carbon nanomaterials such as graphene and CNTs, biomass-derived CNSs are more economical; however, their physicochemical properties are less predictable and difficult to control. High-yield, uniform, and scalable synthesis remains elusive. Importantly, the nature of biomass precursors—such as lignocellulosic residues, algae, and food or municipal waste—plays a decisive role in dictating carbon yield, pore development, heteroatom content, and resulting photocatalytic activity. Lignocellulosic biomass, enriched with cellulose, hemicellulose, and lignin, typically generates CNS with hierarchical porosity and higher structural stability after carbonization, whereas algae- and protein-rich feedstocks inherently introduce nitrogen or sulfur functionalities that can improve charge separation and surface reactivity. In contrast, heterogeneous waste materials often lead to inconsistent ash content and impurity levels, complicating the reproducibility and quality of the final CNS. Therefore, biomass precursor selection directly impacts photocatalytic efficiency, adsorption affinity, and dopant distribution, reinforcing the need for systematic precursor-performance mapping. Moreover, despite being cheaper, biomass-derived CNS must match or exceed the performance of commercial-grade materials like activated carbon or engineered nanocomposites—an expectation that adds further pressure to optimize their structural and surface characteristics [20].

The fabrication of CNS remains a critical bottleneck in advancing its sustainable application, primarily due to the reliance on hazardous reagents, extended reaction durations, and low material yields. Most biomass-derived synthesis protocols still depend on environmentally detrimental chemicals such as H_2SO_4, H_3PO_4, $ZnCl_2$, NaOH, $KMnO_4$, and various heavy metal catalysts [174]. Although these methods aim to valorize waste biomass, their environmental cost often outweighs the benefits of recycling, calling into question the true sustainability of such approaches. As emphasized by Arabpour et al. [175] and Zaib et al. [176], there is an urgent need to transition toward greener, one-pot, and modular synthetic strategies that not only mitigate ecological harm but also offer scalability and practical viability for large-scale CNS production. Ensuring eco-friendliness alongside high material throughput is particularly relevant for biomass-derived CNS, which must retain sustainability as its core advantage. Structurally, tuning the pore architecture of biomass-derived CNS presents a dual-edged challenge. While macroporous 3D architectures—such as foams, aerogels, and spongy frameworks—are advantageous for enhanced mass transfer and light penetration, achieving optimal pore interconnectivity, size distribution, and mechanical stability is complex. Highly porous structures risk compromising structural robustness, especially under variable hydraulic loads in industrial settings. Therefore, future designs must strike a balance between porosity and durability to ensure long-term applicability. Furthermore, material performance under realistic water conditions remains underexplored. In dynamic wastewater matrices, which often contain high levels of natural organic matter (NOM), the selectivity and efficiency of CNS-based photocatalysts can decline sharply. NOM competes with target pollutants for adsorption sites and light absorption, dampening the effectiveness of photocatalytic reactions. This issue is more pronounced in CNS derived from heterogeneous biomass precursors, where inconsistent surface chemistry reduces selectivity. To overcome these drawbacks, future materials should incorporate heteroatom doping (e.g., N, S, P) or composite strategies (e.g., CNS/metal oxide hybrids) to enhance selectivity, surface charge tuning, and catalytic activity under low-intensity light.

From a toxicological perspective, the growing concern over the eco- and cytotoxicity of nanoscale carbon materials must not be overlooked. As CNS particle size decreases and surface reactivity increases, the potential for adverse biological and ecological interactions also rises. Chung et al. [177] emphasized the importance of risk mitigation strategies, particularly for CNTs, which can serve as a blueprint for biomass-derived CNS. Comprehensive life cycle assessments and cytotoxicity assays under environmentally relevant conditions are imperative to validate the safety of these materials. Photostability and reusability are also essential determinants of the long-term feasibility of CNS-based materials. Excessive photoactivity can lead to photocorrosion, reducing the catalytic lifetime and efficiency of the system. Biomass-derived CNS often demonstrate better resistance to photocorrosion compared to pristine graphene or CNTs, likely due to their amorphous nature and inherent defect structures. However, enhancing structural integrity and ensuring recyclability remain critical research priorities. In addition, solubility and dispersibility challenges—particularly in aqueous media—pose obstacles for CNS deployment in flow-through systems. Limited solubility of graphene sheets, CNTs, and graphitic carbon nitride (g-C_3N_4) in water, ethanol, and acetone constrains their uniform distribution, which is essential for efficient pollutant interaction. Biomass-derived CNS must be engineered for improved hydrophilicity, perhaps via surface functionalization or polymer grafting, to facilitate better integration into treatment systems [178, 179]. To guide material innovation, theoretical modeling and computational simulations offer valuable predictive insights. Such tools can streamline the identification of CNS candidates with high adsorption energies, optimal band structures, and surface reactivity, minimizing experimental trial-and-error and focusing efforts on high-potential materials.

Despite the frequent emphasis on biomass-derived CNS as "green" materials, a comprehensive evaluation of their full lifecycle environmental footprint is still insufficiently addressed in current research. A rigorous sustainability assessment must consider upstream and downstream stages—including biomass harvesting, pre-processing, carbonization, doping, operational performance, regeneration, and disposal. For example, although

biomass is renewable, its collection and transport can incur nontrivial energy and carbon costs, especially when sourced from dispersed agricultural or municipal waste streams. Similarly, CNS synthesis routes often involve significant heat input and chemical consumption, which may offset environmental gains when compared to conventional catalysts such as TiO_2 or commercial activated carbon. Therefore, a comparative analysis of energy demands, chemical inputs, and emissions across the full production chain is crucial to validate the claimed sustainability advantages of BMCNS.

End-of-life considerations further influence the true "greenness" of these materials. Catalyst regeneration may require additional thermal or chemical treatments, potentially generating degradation byproducts or secondary waste. Additionally, the fate, persistence, and ecotoxicity of spent CNS—particularly nanoscale fragments—must be evaluated to prevent unintended environmental impacts. Integrating life cycle assessment (LCA), techno-economic analysis (TEA), and ecotoxicological testing would provide a more holistic and realistic sustainability profile for BMCNS [20, 177].

From a commercialization perspective, several practical pathways can accelerate the translation of biomass-derived CNS into viable water treatment technologies:

i. Development of decentralized, modular reactors: Integration of CNS-based photocatalysts into solar-powered, small-scale treatment units can facilitate decentralized water remediation, especially in off-grid or resource-constrained regions [180]. These systems can utilize solar irradiation and gravity-fed flow-through configurations, minimizing energy input and infrastructure requirements.

ii. Industry–academia partnerships: Strong collaborations between academic institutions and water treatment industries can bridge the gap between fundamental research and industrial-scale implementation. Pilot-scale demonstrations, supported by government grants or private investment, can test CNS performance under diverse real-world water matrices and operational conditions [181].

iii. Biomass supply chain optimization: The selection of abundant, low-ash, nitrogen-rich biomass (e.g., algae, agricultural residues, food waste) can reduce synthesis cost and improve CNS doping efficiency [182]. Waste valorization initiatives that align with circular economy models offer mutual benefits for waste management and nanomaterial production.

iv. Green process intensification: Techniques such as microwave-assisted pyrolysis, hydrothermal carbonization, and ionic liquid-based activation offer eco-friendly alternatives to conventional synthesis. These methods enable faster reaction times, lower energy input, and reduced chemical usage, promoting scalability and sustainability [183, 184].

v. Regulatory and safety standardization: Establishing regulatory frameworks for evaluating CNS toxicity, leaching behavior, and environmental fate is essential for public acceptance and commercial certification. Guidelines from agencies like the EPA, ISO, or REACH can provide standardized metrics for risk assessment and material compliance [185].

vi. Hybrid system integration: Incorporating CNS into existing treatment trains—such as combining with membrane filtration, AOPs, or adsorption columns—can boost overall treatment efficacy while reducing the individual limitations of each method. Hybrid systems enable CNS to serve both as primary photocatalysts and synergistic enhancers [186].

In short, while biomass-derived CNS represents a compelling path toward sustainable and effective water treatment solutions, its successful commercialization hinges on overcoming multifaceted challenges related to synthesis, performance optimization, structural design, safety, and scalability. A comprehensive lifecycle sustainability analysis—including resource inputs, operational efficiency, regeneration behavior, waste generation, and ecotoxicity—is essential to substantiate their environmental advantages relative to conventional catalysts. Central to this effort is a clearer understanding of how biomass precursor composition governs the physicochemical and photocatalytic attributes of the resulting CNS—a dimension critical for rational precursor selection and scalable production. Future research must integrate multidisciplinary approaches—combining materials science, environmental engineering, toxicology, and computational modeling—to fully realize the potential of these eco-friendly nanostructures in real-world environmental remediation. By advancing green synthesis methods, validating field performance, and establishing robust commercialization frameworks, biomass-derived CNS can transition from promising laboratory materials to cornerstone components in next-generation water treatment technologies.

7 | Conclusion and Outlook

BMCNSs have garnered significant attention as advanced photocatalytic materials owing to their unique combination of physicochemical versatility and sustainable origin. Their large specific surface area, tunable porosity, high electrical conductivity, and adjustable band gaps collectively contribute to superior photocatalytic efficiency under visible light irradiation. These features facilitate effective charge carrier separation, strong adsorption of organic pollutants, and enhanced catalytic performance—attributes crucial for environmental remediation applications such as wastewater purification. Beyond their functionality, the renewable and carbon-neutral nature of biomass precursors places BMCNSs at the intersection of green chemistry and sustainable development. Converting agricultural residues, forestry by-products, and organic municipal waste into high-value carbon nanostructures transforms low-cost feedstocks into functional materials while reducing waste and environmental burden. Consequently, BMCNSs offer a sustainable and low-impact alternative to conventional photocatalysts like TiO_2, exemplifying a circular approach to resource utilization in line with global environmental and clean energy goals.

Despite notable progress, several challenges remain. The inherent heterogeneity of biomass precursors often leads to inconsistencies in morphology, surface chemistry, and performance, hindering reproducibility and scalability. Energy-intensive synthesis routes, complex activation procedures, and the use of harsh chemical reagents further compromise

sustainability and cost-effectiveness. Moreover, issues related to long-term photochemical and structural stability under realistic environmental conditions persist, limiting large-scale deployment. Addressing these challenges requires an integrated research strategy encompassing scalable synthesis, controlled material design, computational optimization, and thorough safety assessment.

7.1 | Scalable and Eco-Friendly Synthesis

To overcome the challenges of energy-intensive and costly synthesis, developing green, low-cost, and energy-efficient routes is essential for sustainable BMCNS production. Methods such as hydrothermal carbonization, microwave-assisted pyrolysis, and template-free self-assembly provide eco-friendly alternatives to conventional processes. These approaches reduce both chemical waste and operational energy requirements, promoting economic scalability. Green synthetic strategies have demonstrated that biomass-derived nanocomposites can achieve complete dye degradation within minutes under visible light, underscoring the feasibility of coupling sustainability with high catalytic efficiency [187]. Thus, scalable green fabrication directly addresses synthesis cost and energy challenges while preserving high photocatalytic performance.

7.2 | Advanced Material Design and Structural Control

The structural instability and limited recyclability of BMCNSs under prolonged operation can be effectively mitigated through rational nanostructure engineering. Designing hierarchical porous architectures—such as 3D interconnected frameworks, core–shell, and hollow nanostructures—enhances light harvesting, mass transport, and active site accessibility. Furthermore, functionalization strategies, including heteroatom doping (e.g., N, S, B), surface oxidation, and hybridization with semiconductors, allow precise control over electronic and interfacial properties. These modifications strengthen charge transfer dynamics, improve visible-light responsiveness, and enhance durability. For instance, lignin-templated TiO_2 and co-doped carbon composites have achieved superior bandgap tuning, charge separation, and recyclability, enabling rapid pollutant degradation and long-term stability [69, 105]. Therefore, advanced material design directly addresses the challenge of maintaining structural and photochemical stability under realistic conditions.

7.3 | Computational-Experimental Synergy

The heterogeneity of biomass feedstocks remains a critical barrier to reproducibility and optimization. Integrating machine learning (ML) and DFT with experimental studies provides a powerful avenue to overcome this issue. Computational optimization can identify correlations between biomass precursor characteristics (e.g., lignin or cellulose content) and final physicochemical properties, guiding data-driven precursor selection and predictive material design. This synergy enables rational tuning of dopant combinations, electronic structures, and adsorption mechanisms, reducing empirical trial-and-error. Recent computational–experimental workflows have validated the dominant roles of micropore filling, electrostatic interactions, and π–π stacking in adsorption, while guiding the development of nitrogen-doped and biochar-based systems with superior efficiency and sustainability [188, 189]. Hence, computational–experimental integration directly addresses the problem of biomass variability and design complexity.

7.4 | Eco-Toxicological and Environmental Risk Assessment

With the expansion of BMCNS applications into environmental and biomedical domains, the evaluation of ecological and health risks is imperative. Although materials such as graphene and CNTs exhibit outstanding stability and conductivity, their nano–bio interactions may induce oxidative stress, DNA damage, or heavy metal leaching during degradation. Such concerns highlight the necessity for safety-by-design synthesis and multi-tiered risk management strategies. Incorporating exposure monitoring, lifecycle assessment, and adherence to OECD and ECHA regulatory frameworks ensures that the environmental benefits of BMCNSs are realized without unintended ecological consequences [185]. Therefore, eco-toxicological evaluation directly addresses concerns about material safety, sustainability, and public acceptance.

Looking ahead, the convergence of green synthesis, rational nanostructure engineering, computational materials design, and comprehensive risk assessment will be pivotal in advancing BMCNSs toward real-world implementation. By explicitly linking each challenge to its corresponding solution—biomass heterogeneity to computational optimization, synthesis cost and energy intensity to green fabrication, structural instability to advanced material design, and safety risks to eco-toxicological assessment—a cohesive and forward-looking research roadmap can be established. Balancing innovation, performance, and environmental responsibility will enable biomass-derived CNS-based photocatalysts to evolve into transformative materials for sustainable environmental remediation, particularly in the efficient degradation of organic pollutants under visible light irradiation.

Author Contributions

Jagadis Gautam and **Amol M. Kale:** writing – original draft, review and editing. **Jishu Rawal** and **Pooja Varma:** writing – review and editing. **Seung Jun Lee, Seul-Yi Lee** and **Soo-Jin Park:** writing – review and editing, funding acquisition.

Acknowledgments

This work was supported by the Commercialization Promotion Agency for R&D Outcomes (COMPA) grant funded by the Korea government (Ministry of Science and ICT) (RS-2025-2311658) and by the National Research Foundation of Korea (NRF) grant funded by the Korea government (MSIT) (2023R1A2C1004109).

Conflicts of Interest

The authors declare no conflicts of interest.

References

1. A. K. Priya, M. Muruganandam, and S. Suresh, "Bio-Derived Carbon-Based Materials for Sustainable Environmental Remediation and Wastewater Treatment," *Chemosphere* 362 (2024): 142731.

2. S. Qiu, Q. Li, X. Li, et al., "Biomass-Derived Carbon Materials for the Adsorption of Organic Pollutants," *Advanced Sustainable Systems* 8, no. 3 (2024): 2300340.

3. I. Manisalidis, E. Stavropoulou, A. Stavropoulos, and E. Bezirtzoglou, "Environmental and Health Impacts of Air Pollution: A Review," *Frontiers in Public Health* 8 (2020): 14.

4. H. Gomaa, M. Y. Emran, and M. A. El-Gammal, "Biodegradation of Azo Dye Pollutants Using Microorganisms." *Handbook of Biodegradable Materials* (Springer, 2022), 1–29.

5. S. Velusamy, A. Roy, S. Sundaram, and T. Kumar Mallick, "A Review on Heavy Metal Ions and Containing Dyes Removal Through Graphene Oxide-Based Adsorption Strategies for Textile Wastewater Treatment," *Chemical Record* 21, no. 7 (2021): 1570–1610.

6. Z. Liu, X. Huang, Y. Miao, et al., "Eggplant Biomass Based Porous Carbon for Fast and Efficient Dye Adsorption From Wastewater," *Industrial Crops and Products* 187 (2022): 115510.

7. P. Kumari, K. M. Tripathi, K. Awasthi, and R. Gupta, "Biomass-Derived Carbon Nano-Onions for the Effective Elimination of Organic Pollutants and Oils From Water," *Environmental Science and Pollution Research* 30, no. 27 (2023): 71048–71062.

8. K.-C. Chen, J.-Y. Wu, D.-J. Liou, and S.-C. J. Hwang, "Decolorization of the Textile Dyes by Newly Isolated Bacterial Strains," *Journal of Biotechnology* 101, no. 1 (2003): 57–68.

9. M. Ahmed, M. O. Mavukkandy, A. Giwa, et al., "Recent Developments in Hazardous Pollutants Removal From Wastewater and Water Reuse Within a Circular Economy," *npj Clean Water* 5, no. 1 (2022): 12.

10. S. Kato and Y. Kansha, "Comprehensive Review of Industrial Wastewater Treatment Techniques," *Environmental Science and Pollution Research* 31, no. 39 (2024): 51064–51097.

11. A. Jabeen, U. Kamran, S. Noreen, S.-J. Park, and H. N. Bhatti, "Mango Seed-Derived Hybrid Composites and Sodium Alginate Beads for the Efficient Uptake of 2,4,6-Trichlorophenol From Simulated Wastewater," *Catalysts* 12 (2022): 972.

12. H. Wu, L. Li, S. Wang, et al., "Recent Advances of Semiconductor Photocatalysis for Water Pollutant Treatment: Mechanisms, Materials and Applications," *Physical Chemistry Chemical Physics* 25, no. 38 (2023): 25899–25924.

13. K. Prakruthi, M. P. Ujwal, S. R. Yashas, B. Mahesh, N. Kumara Swamy, and H. P. Shivaraju, "Recent Advances in Photocatalytic Remediation of Emerging Organic Pollutants Using Semiconducting Metal Oxides: An Overview," *Environmental Science and Pollution Research* 29, no. 4 (2022): 4930–4957.

14. M. S. Al Ja'farawy, A. Purwanto, and H. Widiyandari, "Carbon Quantum Dots Supported Zinc Oxide (ZnO/CQDs) Efficient Photocatalyst for Organic Pollutant Degradation–A Systematic Review," *Environmental Nanotechnology, Monitoring & Management* 18 (2022): 100681.

15. M. Al Kausor and D. Chakrabortty, "Graphene Oxide Based Semiconductor Photocatalysts for Degradation of Organic Dye in Waste Water: A Review on Fabrication, Performance Enhancement and Challenges," *Inorganic Chemistry Communications* 129 (2021): 108630.

16. K. Rasouli, J. Rasouli, M. S. Mohtaram, et al., "Biomass-Derived Activated Carbon Nanocomposites for Cleaner Production: A Review on Aspects of Photocatalytic Pollutant Degradation," *Journal of Cleaner Production* 419 (2023): 138181.

17. D. A. Giannakoudakis, F. F. Zormpa, A. G. Margellou, et al., "Carbon-Based Nanocatalysts (CnCs) for Biomass Valorization and Hazardous Organics Remediation," *Nanomaterials* 12, no. 10 (2022): 1679.

18. H. He, R. Zhang, P. Zhang, et al., "Functional Carbon From Nature: Biomass-Derived Carbon Materials and the Recent Progress of Their Applications," *Advanced Science* 10, no. 16 (2023): 2205557.

19. A. Vijeata, G. R. Chaudhary, S. Chaudhary, A. A. Ibrahim, and A. Umar, "Recent Advancements and Prospects in Carbon-Based Nanomaterials Derived From Biomass for Environmental Remediation Applications," *Chemosphere* 357 (2024): 141935.

20. R. Wang, Y. Feng, D. Li, K. Li, and Y. Yan, "Towards the Sustainable Production of Biomass-Derived Materials With Smart Functionality: A Tutorial Review," *Green Chemistry* 26 (2024): 9075–9103.

21. J. Arun, N. Nirmala, P. Priyadharsini, et al., "A Mini-Review on Bioderived Carbon and Its Nanocomposites for Removal of Organic Pollutants From Wastewater," *Materials Letters* 310 (2022): 131476.

22. L. Li, Y. Wang, L. Liu, C. Gao, S. Ru, and L. Yang, "Occurrence, Ecological Risk, and Advanced Removal Methods of Herbicides in Waters: A Timely Review," *Environmental Science and Pollution Research* 31, no. 3 (2024): 3297–3319.

23. A. Kumar, A. Thakur, and P. S. Panesar, "A Review on the Industrial Wastewater With the Efficient Treatment Techniques," *Chemical Papers* 77, no. 8 (2023): 4131–4163.

24. A. F. H. Sdiq, H. H. Abdulrahman, H. K. Ismail, et al., "A Review of Effective Nanoadsorbents Made of Carbonaceous, Metal Oxides, and Polymer Nanocomposite Materials for Adsorption of Pharmaceutical Contaminants in Wastewater," *International Journal of Environmental Research* 19, no. 5 (2025): 159.

25. P. Duarah, P. Mondal, P. P. Das, and M. K. Purkait, "Potential of NF Membranes for the Removal of Aquatic Pollutants From Industrial Wastewater: A Review," in *Membrane and Membrane-Based Processes for Wastewater Treatment*, 1st ed. (2023), 1–16.

26. X. Zhao, Y. Liu, Q. Zhu, and W. Gong, "Catechol-Based Porous Organic Polymers for Effective Removal of Phenolic Pollutants From Water," *Polymers* 15, no. 11 (2023): 2565.

27. Z. B. Babar, A. Shahi, A. Rauf, H. Sattar, and K. Rizwan, *Organic–Inorganic Nanohybrids for the Removal of Environmental Pollutants, Hybrid Nanomaterials: Biomedical, Environmental and Energy Applications* (Springer, 2022), 277–309.

28. S. Malik, A. Dhasmana, S. Kishore, and M. Kumari, *Microbes and Microbial Enzymes for Degradation of Pesticides, Bioremediation and Phytoremediation Technologies in Sustainable Soil Management* (Apple Academic Press, 2022), 95–127.

29. N. Nair, V. Gandhi, A. Shukla, S. Ghotekar, V.-H. Nguyen, and K. Varma, "Mechanisms in the Photocatalytic Breakdown of Persistent Pharmaceutical and Pesticide Molecules over TiO_2-based Photocatalysts: A Review," *Journal of Physics: Condensed Matter* 36 (2024): 413003.

30. S. J. Moniz, S. A. Shevlin, D. J. Martin, Z.-X. Guo, and J. Tang, "Visible-Light Driven Heterojunction Photocatalysts for Water Splitting—A Critical Review," *Energy & Environmental Science* 8, no. 3 (2015): 731–759.

31. Z. Shayegan, C.-S. Lee, and F. Haghighat, "TiO_2 Photocatalyst for Removal of Volatile Organic Compounds in Gas Phase–A Review," *Chemical Engineering Journal* 334 (2018): 2408–2439.

32. E. Amdeha, "Biochar-Based Nanocomposites for Industrial Wastewater Treatment via Adsorption and Photocatalytic Degradation and the Parameters Affecting These Processes," *Biomass Conversion and Biorefinery* 14, no. 19 (2024): 23293–23318.

33. A. L. T. Zheng, C. A. C. Abdullah, E. L. T. Chung, and Y. Andou, "Recent Progress in Visible Light-Doped ZnO Photocatalyst for Pollution Control," *International Journal of Environmental Science and Technology* 20, no. 5 (2023): 5753–5772.

34. X. Zhang, W. Li, Y. Lei, J. He, Y. Huang, and W. Tan, "Biomass C-Doped Three-Dimensional Bi_2WO_6 for Enhanced Visible-Light-Driven Photodegradation of Diclofenac and Rhodamine B," *Ceramics International* 50, no. 11 (2024): 18594–18608.

35. J. Lyu, L. Zhou, J. Shao, et al., "TiO_2 Hollow Heterophase Junction With Enhanced Pollutant Adsorption, Light Harvesting, and Charge Separation for Photocatalytic Degradation of Volatile Organic Compounds," *Chemical Engineering Journal* 391 (2020): 123602.

36. Y. Le Thi Hoang Yen, D. Van Thuan, N. T. Hanh, et al., "Synthesis of N and S Co-Doped TiO_2 Nanotubes for Advanced Photocatalytic Degradation of Volatile Organic Compounds (VOCs) in Gas Phase," *Topics in Catalysis* 63 (2020): 1077–1085.

37. S. Saqlain, B. J. Cha, S. Y. Kim, et al., "Impact of Humidity on the Removal of Volatile Organic Compounds Over Fe Loaded TiO_2 Under Visible Light Irradiation: Insight Into Photocatalysis Mechanism by Operando DRIFTS," *Materials Today Communications* 26 (2021): 102119.

38. S. Weon, E. Choi, H. Kim, et al., "Active {001} Facet Exposed TiO_2 Nanotubes Photocatalyst Filter for Volatile Organic Compounds Removal: From Material Development to Commercial Indoor Air Cleaner Application," *Environmental Science & Technology* 52, no. 16 (2018): 9330–9340.

39. E. Amdeha and M. Salem, "Facile Green Synthesis of ZnO Supported on Exfoliated Graphite for Photocatalytic Degradation of Dye under UV and Visible-Light Irradiation," *Egyptian Journal of Chemistry* 65, no. 132 (2022): 557–569.

40. J. Cui, F. Zhang, H. Li, J. Cui, Y. Ren, and X. Yu, "Recent Progress in Biochar-Based Photocatalysts for Wastewater Treatment: Synthesis, Mechanisms, and Applications," *Applied Sciences* 10, no. 3 (2020): 1019.

41. W. Yu, J. Zhang, and T. Peng, "New Insight Into the Enhanced Photocatalytic Activity of N-, C- and S-Doped ZnO Photocatalysts," *Applied Catalysis, B: Environmental* 181 (2016): 220–227.

42. A. Hao, X. Ning, X. Liu, L. Zhan, and X. Qiu, "Phosphorus Heteroatom Doped BiOCl as Efficient Catalyst for Photo-Piezocatalytic Degradation of Organic Pollutant and Unveiling the Mechanism: Experiment and DFT Calculation," *Chemical Engineering Journal* 499 (2024): 155823.

43. K. Shivaji, K. Sridharan, D. D. Kirubakaran, et al., "Biofunctionalized CdS Quantum Dots: A Case Study on Nanomaterial Toxicity in the Photocatalytic Wastewater Treatment Process," *ACS Omega* 8, no. 22 (2023): 19413–19424.

44. D. Chen, H. Zhu, S. Yang, et al., "Micro–Nanocomposites in Environmental Management," *Advanced Materials* 28, no. 47 (2016): 10443–10458.

45. Y. Zhang, J. Chen, Y. Wang, et al., "Cu_2O/Ag-coated Wood-Based Biochar Composites for Efficient Adsorption/Photocatalysis Synergistic Degradation of High-Concentration Azo Dyes," *Applied Surface Science* 647 (2024): 158985.

46. Y. G. Alghamdi, B. Krishnakumar, M. A. Malik, and S. Alhayyani, "Design and Preparation of Biomass-Derived Activated Carbon Loaded TiO_2 Photocatalyst for Photocatalytic Degradation of Reactive Red 120 and Ofloxacin," *Polymers* 14, no. 5 (2022): 880.

47. J. Xiao, J. Han, C. Zhang, G. Ling, F. Kang, and Q. H. Yang, "Dimensionality, Function and Performance of Carbon Materials in Energy Storage Devices," *Advanced Energy Materials* 12, no. 4 (2022): 2100775.

48. H. Luo, C. Ni, C. Zhang, et al., "Lignocellulosic Biomass Derived N-Doped and CoO-Loaded Carbocatalyst Used as Highly Efficient Peroxymonosulfate Activator for Ciprofloxacin Degradation," *Journal of Colloid and Interface Science* 610 (2022): 221–233.

49. B. T. Son, N. V. Long, and N. T. Nhat Hang, "The Development of Biomass-Derived Carbon-Based Photocatalysts for the Visible-Light-Driven Photodegradation of Pollutants: A Comprehensive Review," *RSC Advances* 11, no. 49 (2021): 30574–30596.

50. P. Sinha, A. Yadav, A. Tyagi, et al., "Keratin-Derived Functional Carbon With Superior Charge Storage and Transport for High-Performance Supercapacitors," *Carbon* 168 (2020): 419–438.

51. S. Choy, H. T. Bui, D. Van Lam, S. M. Lee, W. Kim, and D. S. Hwang, "Photocatalytic Exoskeleton: Chitin Nanofiber for Retrievable and Sustainable TiO_2 Carriers for the Decomposition of Various Pollutants," *Carbohydrate Polymers* 271 (2021): 118413.

52. F. Liang, J. Cui, C. Ning, et al., "Construction of Biomass-Derived Magnetic-Recyclable FeNi-LDO@CS to Activate Persulfate for Simultaneous Degradation of Cationic and Anionic Dyes: Discrepancy, Mechanism and Toxicity Analysis," *Journal of Environmental Sciences* 154 (2025): 741–759.

53. K. Cheng, W. Shao, H. Li, et al., "Biomass Derived Carbon Dots Mediated Exciton Dissociation in Rose Flower-Like Carbon Nitride for Boosting Photocatalytic Performance," *Industrial Crops and Products* 192 (2023): 116086.

54. I. Fatimah, N. I. Prakoso, I. Sahroni, et al., "Physicochemical Characteristics and Photocatalytic Performance of TiO_2/SiO_2 Catalyst Synthesized Using Biogenic Silica From Bamboo Leaves," *Heliyon* 5, no. 11 (2019): e02766.

55. W. Tian, H. Sun, X. Duan, H. Zhang, Y. Ren, and S. Wang, "Biomass-Derived Functional Porous Carbons for Adsorption and Catalytic Degradation of Binary Micropollutants in Water," *Journal of Hazardous Materials* 389 (2020): 121881.

56. Y. Wang, S. Wang, T. Xie, and J. Cao, "Activated Carbon Derived From Waste Tangerine Seed for the High-Performance Adsorption of Carbamate Pesticides From Water and Plant," *Bioresource Technology* 316 (2020): 123929.

57. W. Wang and M. Chen, "Catalytic Degradation of Sulfamethoxazole by Peroxymonosulfate Activation System Composed of Nitrogen-Doped Biochar From Pomelo Peel: Important Roles of Defects and Nitrogen, and Detoxification of Intermediates," *Journal of Colloid and Interface Science* 613 (2022): 57–70.

58. B. Chu, Y. Lou, Y. Tan, J. Lin, and X. Liu, "Nitrogen-Doped Mesoporous Activated Carbon From Lentinus Edodes Residue: An Optimized Adsorbent for Pharmaceuticals in Aqueous Solutions," *Frontiers in Chemistry* 12 (2024): 1419287.

59. J. Cheng, J.-J. Gu, W. Tao, et al., "Edible Fungus Slag Derived Nitrogen-Doped Hierarchical Porous Carbon as a High-Performance Adsorbent for Rapid Removal of Organic Pollutants From Water," *Bioresource Technology* 294 (2019): 122149.

60. H. Meng, C. Nie, W. Li, et al., "Insight Into the Effect of Lignocellulosic Biomass Source on the Performance of Biochar as Persulfate Activator for Aqueous Organic Pollutants Remediation: Epicarp and Mesocarp of Citrus Peels as Examples," *Journal of Hazardous Materials* 399 (2020): 123043.

61. S. Nath, A. Naha, K. Saikia, C. P. Choudhury, and V. Venkatramanan, "Degradation of Organic Pollutants Using Lignin-Derived Carbon Materials as a Sustainable Approach to Environmental Remediation," *Biotechnology for Sustainable Materials* 2, no. 1 (2025): 11.

62. L. A. González Fernández, N. A. Medellín Castillo, M. Sánchez Polo, A. E. Navarro Frómeta, and J. E. Vilasó Cadre, "Algal-Based Carbonaceous Materials for Environmental Remediation: Advances in Wastewater Treatment, Carbon Sequestration, and Biofuel Applications," *Processes* 13, no. 2 (2025): 556.

63. R. Chakraborty, V. K, M. Pradhan, and A. K. Nayak, "Recent Advancement of Biomass-Derived Porous Carbon Based Materials for Energy and Environmental Remediation Applications," *Journal of Materials Chemistry A* 10, no. 13 (2022): 6965–7005.

64. M. Wang, H. Zhou, and F. Wang, "Photocatalytic Biomass Conversion for Hydrogen and Renewable Carbon-Based Chemicals," *Joule* 8, no. 3 (2024): 604–621.

65. U. Kamran, H. N. Bhatti, S. Noreen, M. A. Tahir, and S.-J. Park, "Chemically Modified Sugarcane Bagasse-Based Biocomposites for Efficient Removal of Acid Red 1 Dye: Kinetics, Isotherms, Thermodynamics, and Desorption Studies," *Chemosphere* 291 (2022): 132796.

66. H. Liu, J. Long, K. Zhang, et al., "Agricultural Biomass/Waste-Based Materials Could be a Potential Adsorption-Type Remediation Contributor to Environmental Pollution Induced by Pesticides—A Critical Review," *Science of the Total Environment* 946 (2024): 174180.

67. M. M. Ansari, Y. Heo, K. Do, M. Ghosh, and Y.-O. Son, "Nanocellulose Derived From Agricultural Biowaste By-Products–Sustainable Synthesis, Biocompatibility, Biomedical Applications, and Future Perspectives: A Review," *Carbohydrate Polymer Technologies and Applications* 8 (2024): 100529.

68. U. Kamran and S.-J. Park, "MnO_2-decorated Biochar Composites of Coconut Shell and Rice Husk: An Efficient Lithium Ions Adsorption-Desorption Performance in Aqueous Media," *Chemosphere* 260 (2020): 127500.

69. Y. Mu, S. Yang, Y. Li, et al., "Highly Efficient Adsorptive and Photocatalytic Degradation of Dye Pollutants Over Biomass-Derived Carbon-Supported Ag Composites Under Visible Light," *Journal of Environmental Chemical Engineering* 9, no. 6 (2021): 106580.

70. R. Shakunthala, C. Sivaa Vignesh, R. Viswanathan, and M. Matheswaran, "Solar Photocatalytic Process Using Biomass-Derived Boron Carbon Nitride (BM-BCN) for the Treatment of Synthetic Textile Effluent," *Catalysis Today* 432 (2024): 114583.

71. S. Ullah, O. P. Kumar, R. Ali, et al., "Biomass Derived Hybrid Activated Carbon/Iron Oxide Composite for Photodegradation of Methylene Blue Upon Visible Light," *ChemistrySelect* 10, no. 7 (2025): e202405028.

72. H. Ding, Z. Liu, Q. Zhang, et al., "Biomass Porous Carbon as the Active Site to Enhance Photodegradation of Oxytetracycline on Mesoporous gC 3 N 4," *RSC Advances* 12, no. 3 (2022): 1840–1849.

73. D. Su, W. Xu, D. Yang, et al., "In Situ Growth of ZnAl-LDH on Biomass Carbon for Highly Efficient Photodegradation of Malachite Green (MG) From Water," *Applied Organometallic Chemistry* 39, no. 1 (2025): e7942.

74. H. Li, C. He, A. Xiao, Y. Hu, L. Luo, and F. Jiang, "Dye-Sensitization on Rosette-Shaped Biobr/Biochar Photocatalyst for Simultaneous Removal of Emerging Pollutants and Dyes," *Journal of Cleaner Production* 469 (2024): 143239.

75. K. P. Sahu and S. Banerjee, "Metal-Free Degradation of Methyl Orange: Unprecedented Catalytic Efficiency of Rice Husk-Derived Graphitic Carbon," *Discover Materials* 5, no. 1 (2025): 141.

76. L. Xu, B. Fu, Y. Sun, et al., "Degradation of Organic Pollutants by Fe/N Co-Doped Biochar via Peroxymonosulfate Activation: Synthesis, Performance, Mechanism and Its Potential for Practical Application," *Chemical Engineering Journal* 400 (2020): 125870.

77. Y. L. Pang, A. Z. Y. Koe, Y. Y. Chan, S. Lim, and W. C. Chong, "Enhanced Sonocatalytic Performance of Non-Metal Graphitic Carbon Nitride ($g\text{-}C_3N_4$)/Coconut Shell Husk Derived-Carbon Composite," *Sustainability* 14, no. 6 (2022): 3244.

78. P. Dong, K. Gao, L. Zhang, et al., "Hydrogen Bond-Assisted Construction of MOF/Semiconductor Heterojunction Photocatalysts for Highly Efficient Electron Transfer," *Applied Catalysis B: Environment and Energy* 357 (2024): 124297.

79. L. Zhang, X. Lu, J. Sun, C. Wang, and P. Dong, "Insights Into the Plasmonic 'Hot Spots' and Efficient Hot Electron Injection Induced by Ag Nanoparticles in a Covalent Organic Framework for Photocatalytic H_2 Evolution," *Journal of Materials Chemistry A* 12, no. 9 (2024): 5392–5405.

80. Y. Li, W. Wang, L. Chen, et al., "Visible-Light-Driven Z-Type Pg-C_3N_4/Nitrogen Doped Biochar/$BiVO_4$ Photo-Catalysts for the Degradation of Norfloxacin," *Materials* 17, no. 7 (2024): 1634.

81. Y. Zhong, X. Zhang, Y. Wang, X. Zhang, and X. Wang, "Carbon Quantum Dots From Tea Enhance Z-Type $BiOBr/C_3N_4$ Heterojunctions for RhB Degradation: Catalytic Effect, Mechanisms, and Intermediates," *Applied Surface Science* 639 (2023): 158254.

82. Y. Cheng, J. Chen, P. Wang, et al., "Interfacial Engineering Boosting the Piezocatalytic Performance of Z-Scheme Heterojunction for Carbamazepine Degradation: Mechanism, Degradation Pathway and DFT Calculation," *Applied Catalysis, B: Environmental* 317 (2022): 121793.

83. J. Pan, A. Zhang, L. Zhang, and P. Dong, "Construction of S-Scheme Heterojunction From Protonated DA Typed Polymer and MoS_2 for Efficient Photocatalytic H_2 Production," *Chinese Journal of Catalysis* 58 (2024): 180–193.

84. P. Singh, N. Rani, S. Kumar, et al., "Assessing the Biomass-Based Carbon Dots and Their Composites for Photocatalytic Treatment of Wastewater," *Journal of Cleaner Production* 413 (2023): 137474.

85. Z. Hu, Z. Shen, and J. C. Yu, "Converting Carbohydrates to Carbon-Based Photocatalysts for Environmental Treatment," *Environmental Science & Technology* 51, no. 12 (2017): 7076–7083.

86. D. Polidoro, A. Perosa, M. Selva, and D. Rodríguez-Padrón, "Metal-Free Carbonaceous Catalytic Materials: Biomass Feedstocks for a Greener Future," *ChemCatChem* 15, no. 13 (2023): e202300415.

87. A. Qurtulen and A. Ahmad, "Green Tea Waste–Derived Carbon Dots: Efficient Degradation of RhB Dye and Selective Sensing of Cu^{2+} Ions," *Environmental Science and Pollution Research* 30, no. 58 (2023): 121630–121646.

88. S. Hong, A. Wei, C. Xie, X. Shen, J.-L. Wen, and T.-Q. Yuan, "Des-Driven Sustainable Dual Valorization of Lignocellulose into Carbon Dots and Porous Biochar for Effective Wastewater Remediation," *International Journal of Biological Macromolecules* 282 (2024): 137159.

89. K. C. Hui, W. L. Ang, and N. S. Sambudi, "Nitrogen and Bismuth-Doped Rice Husk-Derived Carbon Quantum Dots for Dye Degradation and Heavy Metal Removal," *Journal of Photochemistry and Photobiology, A: Chemistry* 418 (2021): 113411.

90. M. Baruah, S. L. Ezung, S. Sharma, U. Bora Sinha, and D. Sinha, "Synthesis and Characterization of Ni-Doped TiO_2 Activated Carbon Nanocomposite for the Photocatalytic Degradation of Anthracene," *Inorganic Chemistry Communications* 144 (2022): 109905.

91. Z. Hu, Y. Huang, X. He, W. Guo, and K. Yan, "Solution-Phase Conversion of Glucose Into Semiconductive Carbonaceous Nanosheet Photocatalysts for Enhanced Environmental Applications," *Chemical Engineering Journal* 427 (2022): 131464.

92. R. Montazeri, Z. Barbari, H. Hosseini-Monfared, and Y. Mohammadi, "Lignin-Derived Carbon and Activated Carbon Nanocomposites With TiO2 as Enhanced Photocatalysts for Organic Pollutant Degradation," *Journal of Nanoparticle Research* 26, no. 8 (2024): 191.

93. S. Begum and M. Ahmaruzzaman, "Biogenic Synthesis of SnO_2/Activated Carbon Nanocomposite and Its Application as Photocatalyst in the Degradation of Naproxen," *Applied Surface Science* 449 (2018): 780–789.

94. I. Khan, M. Sadiq, I. Khan, and K. Saeed, "Manganese Dioxide Nanoparticles/Activated Carbon Composite as Efficient UV and Visible-Light Photocatalyst," *Environmental Science and Pollution Research* 26 (2019): 5140–5154.

95. M. Vinayagam, S. Ramachandran, V. Ramya, and A. Sivasamy, "Photocatalytic Degradation of Orange G Dye Using ZnO/Biomass Activated Carbon Nanocomposite," *Journal of Environmental Chemical Engineering* 6, no. 3 (2018): 3726–3734.

96. T. B. Devi, D. Mohanta, and M. Ahmaruzzaman, "Biomass Derived Activated Carbon Loaded Silver Nanoparticles: An Effective Nanocomposites for Enhanced Solar Photocatalysis and Antimicrobial Activities," *Journal of Industrial and Engineering Chemistry* 76 (2019): 160–172.

97. N. Dhiman, V. K. Tripathi, J. Dwivedi, R. K. Gupta, and K. M. Tripathi, "Photoactive Graphene Aerogel From Biomass for the Visible-Light-Induced Degradation of Pharmaceutical Residues," *ACS Sustainable Resource Management* 1, no. 6 (2024): 1068–1075.

98. L. Han, P. Zhang, L. Li, et al., "Nitrogen-Containing Carbon Nano-Onions-Like and Graphene-Like Materials Derived From Biomass and the Adsorption and Visible Photocatalytic Performance," *Applied Surface Science* 543 (2021): 148752.

99. M. Wu, Y. Tao, Y. Liu, et al., "Fe-N-Coordinated Graphene-Like Honeycomb Porous Carbon as an Extremely Effective Catalyst for Catalytic Oxidation," *Separation and Purification Technology* 354 (2025): 129225.

100. K. Gupta, D. Gupta, and O. P. Khatri, "Graphene-Like Porous Carbon Nanostructure From Bengal Gram Bean Husk and Its Application for Fast and Efficient Adsorption of Organic Dyes," *Applied Surface Science* 476 (2019): 647–657.

101. G. Zeng, H. Zhang, S. Liang, et al., "Highly Efficient Photocatalytic Degradation of the Emerging Pollutant Ciprofloxacin via the Rational Design of a Magnetic Interfacial Junction of Mangosteen Peel Waste-Derived 3D Graphene Hybrid Material," *Environmental Science: Nano* 9, no. 4 (2022): 1298–1314.

102. Q. Zhou, L. Qin, H. Liu, et al., "Microwave Assisted Biomass Derived Carbon Aerogel for Highly Efficient Oxytetracycline Hydrochloride Degradation: Singlet Oxygen Mechanism and C Vacancies Accelerated Electron Transfer," *Chemical Engineering Journal* 487 (2024): 150370.

103. M. V. Arularasu, M. Y. Begum, A. Alamri, and A. A. Fatease, "Visible Light Degradation of Antibiotics Catalyzed by Nanoporous carbon/V2O5 Nanocomposite: Structural, Optical and Electrochemical Properties," *Journal of Molecular Structure* 1322 (2025): 140615.

104. M. M. G. Pastre, D. L. Cunha, A. Kuznetsov, B. S. Archanjo, and M. Marques, "Optimization of Methylene Blue Removal From Aqueous Media by Photocatalysis and Adsorption Processes Using Coconut Biomass-Based Composite Photocatalysts," *Water, Air, & Soil Pollution* 235, no. 3 (2024): 207.

105. W. Zhang, Y. Liang, C. Hu, et al., "3D Structure-Functional Design of a Biomass-Derived Photocatalyst for Antimicrobial Efficacy and Chemical Degradation Under Ambient Conditions," *Green Chemistry* 26, no. 19 (2024): 10139–10151.

106. M. Abdullah, J. Iqbal, M. S. Ur Rehman, et al., "Removal of Ceftriaxone Sodium Antibiotic From Pharmaceutical Wastewater Using an Activated Carbon Based TiO_2 Composite: Adsorption and Photocatalytic Degradation Evaluation," *Chemosphere* 317 (2023): 137834.

107. H. Kadkhodayan and T. Alizadeh, "Fabrication of High-Performance Multifunctional Fe-Doped La_2ZnTiO_6 Double Perovskite/Activated Carbon Nanocomposite for Efficient Photocatalytic Degradation of Dyes, Nitrate and Carbon Dioxide Pollutants," *Materials Today Chemistry* 26 (2022): 101034.

108. S. Luo, C. Liu, S. Zhou, et al., "ZnO Nanorod Arrays Assembled on Activated Carbon Fibers for Photocatalytic Degradation: Characteristics and Synergistic Effects," *Chemosphere* 261 (2020): 127731.

109. S. N. U. S. Bukhari, A. A. Shah, W. Liu, et al., "Activated Carbon Based TiO2 Nanocomposites (TiO2@ Ac) Used Simultaneous Adsorption and Photocatalytic Oxidation for the Efficient Removal of Rhodamine-B (Rh–B)," *Ceramics International* 50, no. 21 (2024): 41285–41298.

110. S. L. Ezung, M. Baruah, S. Sharma, et al., "Photocatalytic Degradation of Chlorpyrifos Using Fe-Doped ZnO/Activated Carbon Nanocomposite," *Journal of Molecular Structure* 1319 (2025): 139434.

111. B. Albiss and M. Abu-Dalo, "Photocatalytic Degradation of Methylene Blue Using Zinc Oxide Nanorods Grown on Activated Carbon Fibers," *Sustainability* 13, no. 9 (2021): 4729.

112. P. Shanmugam, B. Parasuraman, S. Boonyuen, et al., "Hydrothermal Synthesis and Photocatalytic Application of ZnS-Ag Composites Based on Biomass-Derived Carbon Aerogel for the Visible Light Degradation of Methylene Blue," *Environmental Geochemistry and Health* 46, no. 3 (2024): 92.

113. S. Park, J. Kim, and K. Kwon, "A Review on Biomass-Derived N-Doped Carbons as Electrocatalysts in Electrochemical Energy Applications," *Chemical Engineering Journal* 446 (2022): 137116.

114. A. Khan, M. Goepel, J. C. Colmenares, and R. Gläser, "Chitosan-Based N-Doped Carbon Materials for Electrocatalytic and Photocatalytic Applications," *ACS Sustainable Chemistry & Engineering* 8, no. 12 (2020): 4708–4727.

115. L.-H. Kong, Y. Wu, R.-F. Shen, et al., "Combination of N-Doped Porous Carbon and g-C_3N_4 for Effective Removal of Organic Pollutants via Activated Peroxymonosulfate," *Journal of Environmental Chemical Engineering* 10, no. 3 (2022): 107808.

116. S. Kumbhar and M. De, "Waste Biomass Derived Nitrogen-Rich Carbon Dots Augmented g-C_3N_4 Photocatalyst for Valorization of Glycerol," *Materials Science and Engineering: B* 298 (2023): 116815.

117. Y. Wang, Y. Chen, Q. Meng, et al., "Supramolecular Imprinted Cellulose-Based N-Doped Biomass Carbon Fiber for Visual Detection and Specific Degradation of Perfluorooctanoic Acid," *Separation and Purification Technology* 332 (2024): 125824.

118. A. Marpongahtun, Y. Andriayani, Y. Muis, et al., "Biomass-Derived N-Doped Carbon Dots/TiO_2 for Visible-Light-Induced Degradation of Methyl Orange in Wastewater," *Chemistry Africa* 7, no. 6 (2024): 3319–3328.

119. K. Zheng and L. Xiao, "Iron and Nitrogen Co-Doped Porous Carbon Derived From Natural Cellulose of Wood Activating Peroxymonosulfate for Degradation of Tetracycline: Role of Delignification and Mechanisms," *International Journal of Biological Macromolecules* 222 (2022): 2041–2053.

120. C. Wu, J. Zhang, B. Fang, et al., "Self-Floating Biomass Charcoal Supported Flower-Like Plasmon Silver/Carbon, Nitrogen Co-Doped Defective TiO2 as Robust Visible Light Photocatalysts," *Journal of Cleaner Production* 329 (2021): 129723.

121. Y. Zhang, G. Zhao, L. Gan, H. Lian, and M. Pan, "S-Doped Carbon Nanosheets Supported ZnO With Enhanced Visible-Light Photocatalytic Performance for Pollutants Degradation," *Journal of Cleaner Production* 319 (2021): 128803.

122. Y. Lan, Y. Luo, S. Yu, et al., "Cornstalk Hydrochar Produced by Phosphoric Acid-Assisted Hydrothermal Carbonization for Effective Adsorption and Photodegradation of Norfloxacin," *Separation and Purification Technology* 330 (2024): 125543.

123. T. Wang, L. Xue, L. Zheng, et al., "Biomass-Derived N/S Dual-Doped Hierarchically Porous Carbon Material as Effective Adsorbent for the Removal of Bisphenol F and Bisphenol S," *Journal of Hazardous Materials* 416 (2021): 126126.

124. Z. Zhu, P. Yang, X. Li, et al., "Green Preparation of Palm Powder-Derived Carbon Dots Co-Doped With Sulfur/Chlorine and Their Application in Visible-Light Photocatalysis," *Spectrochimica Acta, Part A: Molecular and Biomolecular Spectroscopy* 227 (2020): 117659.

125. S. Liu, Q. Li, S. Zuo, and H. Xia, "Facile Synthesis of Lignosulfonate-Derived Sulfur-Doped Carbon Materials for Photocatalytic Degradation of Tetracycline Under Visible-Light Irradiation," *Microporous and Mesoporous Materials* 336 (2022): 111876.

126. R. Sharma, J. Thakur, V. B. Jaryal, et al., "Nitrogen and Sulfur Functionalized Microporous Carbon Nanomaterial Derived From Waste Coconut Husk for the Efficient Detection and Removal of Ofloxacin," *Chemosphere* 346 (2024): 140653.

127. S. Tong, Y. Lin, Y. Zhang, J. Nie, X. Li, and C. Yang, "Boosting Photocatalytic Performance of Silver Phosphate via Coupling With P-Doped Carbon for Amoxicillin Degradation," *Colloids and Surfaces, A: Physicochemical and Engineering Aspects* 680 (2024): 132653.

128. C. Yu, J. Dan, Z. Liu, et al., "A Facile, Green Strategy to Synthesize N/P Self-Doped, Biomass-Derived, Hierarchical Porous Carbon From Water Hyacinth for Efficient VOCs Adsorption," *Fuel* 358 (2024): 130136.

129. I. H. Alsohaimi, "Novel Synthesis of Polystyrenesulfonate@ AC Based on Olive Tree Leaves Biomass for the Photo-Degradation of Methylene Blue From Aqueous Solution," *Polymers* 16, no. 23 (2024): 3321.

130. J. Matos, P. S. Poon, R. Montaña, et al., "Photocatalytic Activity of P-Fe/Activated Carbon Nanocomposites Under Artificial Solar Irradiation," *Catalysis Today* 356 (2020): 226–240.

131. X. Wei, X. Zhang, L. Jin, et al., "Waste Biomass-Derived Biochar in Adsorption-Photocatalytic Conversion of CO_2 for Sustainable Energy and Environment: Evaluation, Mechanism, and Life Cycle Assessment," *Applied Catalysis B: Environment and Energy* 351 (2024): 123957.

132. S. Sutar, S. Otari, and J. Jadhav, "Biochar Based Photocatalyst for Degradation of Organic Aqueous Waste: A Review," *Chemosphere* 287 (2022): 132200.

133. U. Kamran, S.-Y. Lee, K. Y. Rhee, and S.-J. Park, "Rice Husk Valorization Into Sustainable Ni@ TiO_2/Biochar Nanocomposite for Highly Selective Pb (II) Ions Removal From an Aqueous Media," *Chemosphere* 323 (2023): 138210.

134. D. Zheng, Y. Wang, X. Jia, et al., "Developing Prussian Blue/Wood-Derived Biochar Catalyst for Persistent Organic Pollutant Degradation: Preparation, Characterization, and Mechanism," *Chemosphere* 351 (2024): 141150.

135. J. Kuan, H. Zhang, H. Gu, Y. Zhang, H. Wu, and N. Mao, "Adsorption-Enhanced Photocatalytic Property of Ag-Doped Biochar/g-C_3N_4/TiO_2 Composite by Incorporating Cotton-Based Biochar," *Nanotechnology* 33, no. 34 (2022): 345402.

136. S. Xin, S. Huo, C. Zhang, et al., "Coupling Nitrogen/Oxygen Self-Doped Biomass Porous Carbon Cathode Catalyst With $CuFeO_2$/Biochar Particle Catalyst for the Heterogeneous Visible-Light Driven Photo-Electro-Fenton Degradation of Tetracycline," *Applied Catalysis, B: Environmental* 305 (2022): 121024.

137. C. Wang, R. Sun, and R. Huang, "Highly Dispersed Iron-Doped Biochar Derived From Sawdust for Fenton-Like Degradation of Toxic Dyes," *Journal of Cleaner Production* 297 (2021): 126681.

138. R. Kumar, S. Sharma, N. Kumari, et al., "Biomass-Derived Biochar and Cuo–NiO Nanocomposites: Eco-Friendly Solutions for Environmental Cleanup," *International Journal of Environmental Research* 19, no. 1 (2025): 26.

139. N. P. F. Gonçalves, M. A. O. Lourenço, S. R. Baleuri, S. Bianco, P. Jagdale, and P. Calza, "Biochar Waste-Based ZnO Materials as Highly Efficient Photocatalysts for Water Treatment," *Journal of Environmental Chemical Engineering* 10, no. 2 (2022): 107256.

140. V. Soni, P. Sonu, P. Singh, et al., "Fabricating Cattle Dung-Derived Nitrogen-Doped Biochar Supported Oxygen-Deficient ZnO and Cu_2O-based Novel Step-Scheme Photocatalytic System for Aqueous Doxycycline Hydrochloride Mitigation and Cr (VI) Reduction," *Journal of Environmental Chemical Engineering* 11, no. 5 (2023): 110856.

141. W. Wang, J. Zhang, T. Chen, et al., "Preparation of TiO_2-modified Biochar and Its Characteristics of Photo-Catalysis Degradation for Enrofloxacin," *Scientific Reports* 10, no. 1 (2020): 6588.

142. P. Eswaran, P. D. Madasamy, K. Pillay, and H. Brink, "Sunlight-Driven Photocatalytic Degradation of Methylene Blue Using ZnO/Biochar Nanocomposite Derived From Banana Peels," *Biomass Conversion and Biorefinery* 15 (2024): 1–21.

143. M. S. Mohtaram, S. Mohtaram, S. Sabbaghi, et al., "Photocatalytic Degradation of Acetaminophen Using a Novel TiO_2-Orange Peel-Derived Biochar Composite: Synthesize, Characterization and Optimization of Key Factors," *Journal of Water Process Engineering* 58 (2024): 104884.

144. W. Liu, C. Jiang, J. Feng, L. Zhang, Q. Hou, and X. Ji, "Enhancing Photocatalytic Destruction of Lignin via Cellulose Derived Carbon Quantum Dots/g-C_3N_4 Heterojunctions," *International Journal of Biological Macromolecules* 260 (2024): 129587.

145. S. G. Kumbhar and M. De, "Selective Oxidation of Glycerol to Value-Added Chemicals Over Green Carbon Dots Modified Graphitic Carbon Nitride Charge-Transfer Photocatalyst," *Emergent Materials* 8 (2024): 1–19.

146. X. Gao, L. Sun, P. Hao, et al., "Construction of Black g-C_3N_4/Loofah/Chitosan Hydrogel as an Efficient Solar Evaporator for Desalination Coupled With Antibiotic Degradation," *Separation and Purification Technology* 355 (2025): 129615.

147. C. Cheng, H. Jing, H. Ji, Y. Li, L. Ma, and J. Hao, "Bioderived Carbon Aerogels Loaded With g-C_3N_4 and Their High Efficacy Removing Volatile Organic Compounds (VOCs)," *Journal of Colloid and Interface Science* 678 (2025): 1112–1121.

148. L. Wu, Y. Chen, Y. Li, Q. Meng, and T. Duan, "Functionally Integrated g-C_3N_4@Wood-derived Carbon With an Orderly Interconnected Porous Structure," *Applied Surface Science* 540 (2021): 148440.

149. L. Wu, Y. Chen, Y. Li, Q. Meng, and T. Duan, "Functionally Integrated g-C_3N_4@ Wood-Derived Carbon With an Orderly Interconnected Porous Structure," *Applied Surface Science* 540 (2021): 148440.

150. F. Tang, J. Tang, D. Wang, C. Deng, S. Li, and X. Yang, "Synthesis of Molybdenum Trioxide/Graphite Carbon Nitride Heterojunction Modified by Biomass Carbon Dots and Its Application in Photocatalytic Degradation of Methylene Blue," *Diamond and Related Materials* 137 (2023): 110078.

151. J. Yang, W. Yang, C. Zhang, et al., "Synergistic Self-Driven and Heterogeneous Effect of a Biomass-Derived Urchin-Like Mn_3O_4/C_3N_4 Janus Micromotor Catalyst for Efficient Degradation of Carbamazepine," *RSC Advances* 14, no. 39 (2024): 28904–28914.

152. N. Arif, Y. Ma, M. N. Zafar, et al., "Design and Fabrication of Biomass Derived Black Carbon Modified g-C_3N_4/$FeIn_2S_4$ Heterojunction as Highly Efficient Photocatalyst for Wastewater Treatment," *Small* 20, no. 20 (2024): 2308908.

153. V. L. Chandraboss, J. Kamalakkannan, and S. Senthilvelan, "Synthesis of Activated Charcoal Supported Bi-Doped TiO_2 Nanocomposite Under Solar Light Irradiation for Enhanced Photocatalytic Activity," *Applied Surface Science* 387 (2016): 944–956.

154. S. Chaiwichian, "Synthesis of Novel Activated carbon/BiVO4 nanocomposite photocatalysts for degradation of organic compounds in wastewater." *Journal of Physics: Conference Series* (IOP Publishing, 2022), 012002.

155. T. Wang, X. Liu, D. Han, et al., "Biomass Derived the V-Doped Carbon/Bi_2O_3 Composite for Efficient Photocatalysts," *Environmental Research* 182 (2020): 108998.

156. J. Rasouli, M. Binazadeh, and S. Sabbaghi, "Synthesis of a Novel Biomass Waste-Based Photocatalyst for Degradation of High Concentration Organic Pollutants Under Visible Light: Optimization of Synthesis Condition and Operational Parameters via RSM-CCD," *Surfaces and Interfaces* 49 (2024): 104400.

157. A. MariaJoseph, M. Okhawilai, S. Rajendran, and P. Pattananuwat, "Waste Lignocellulosic Biomass-Derived Graphitic Carbon Encased Bimetallic Nickel-Palladium Oxide Nanofibers for Efficient Organic Dye Pollutant Removal and Antibacterial Actions," *International Journal of Biological Macromolecules* 284 (2025): 137655.

158. H. Pokkiladathu, S. Farissi, A. Sakkarai, and M. Muthuchamy, "Degradation of Bisphenol A: A Contaminant of Emerging Concern, Using Catalytic Ozonation by Activated Carbon Impregnated Nanocomposite-Bimetallic Catalyst," *Environmental Science and Pollution Research* 29, no. 48 (2022): 72417–72430.

159. S. S. P. Selvin, A. G. Kumar, L. Sarala, et al., "Photocatalytic Degradation of Rhodamine B Using Zinc Oxide Activated Charcoal Polyaniline Nanocomposite and Its Survival Assessment Using Aquatic Animal Model," *ACS Sustainable Chemistry & Engineering* 6, no. 1 (2018): 258–267.

160. X. Li, Z. Yang, G. Wu, et al., "Fabrication of Ultrathin Lily-Like $NiCo_2O_4$ Nanosheets via Mooring NiCo Bimetallic Oxide on Waste Biomass-Derived Carbon for Highly Efficient Removal of Phenolic Pollutants," *Chemical Engineering Journal* 441 (2022): 136066.

161. S. Zhang, R. Wang, J. Zhu, et al., "Two-Step Synthesis of Coconut Shell Biochar-Based Ternary Composite to Efficiently Remove Organic Pollutants by Photocatalytic Degradation," *Journal of Environmental Chemical Engineering* 12, no. 3 (2024): 112963.

162. S. M. Roopan, S. H. Prakash, R. Manjupriya, et al., "Biomass-Derived Carbon Quantum Dots-Supported Metal Oxide Composite for the Photocatalytic Degradation of Toxic Pollutants," *Biomass Conversion and Biorefinery* 15 (2024): 1–20.

163. N. S. K. Parambil, S. J. Raphael, P. Joseph, T. Prakash, I. H. Joe, and A. Dasan, "Eco-Friendly TiO_2/CQDs Nanocomposites From Banana Peel Waste: Innovations in Visible Light Induced Organic Pollutant Degradation and X-Ray Shielding Applications," *Biomass Conversion and Biorefinery* 15 (2024): 1–20.

164. Q. Si, W. Guo, H. Wang, et al., "Bio-CQDs Surface Modification BiOCl for the BPA Elimination and Evaluation in Visible Light: The Contribution of C-Localized Level," *Journal of Colloid and Interface Science* 602 (2021): 1–13.

165. E. S. Paghaleh, K. Dashtian, J. Y. Seyf, F. Seidi, and E. Kolvari, "Green Synthesis of Stable $CuFe_2O_4$/CuO-rGO Heterostructure Photocatalyst Using Basil Seeds as Chemo-Reactors for Improved Oxytetracycline Degradation," *Journal of Environmental Chemical Engineering* 11, no. 5 (2023): 110676.

166. D. Negoescu, V. Bratan, M. Gherendi, et al., "Iron Promoted TiO_2-Activated Carbon Nanocomposites for Photocatalytic Degradation of Congo Red in Water," *Catalysts* 14, no. 12 (2024): 844.

167. H. Wu, S. Luo, H. Wang, et al., "An Ultra-Stable Sodium Dual-Ion Battery Based on S/Se Co-Doped Covalent Organic Framework Anode With 12,000 Cycles Under Lean Electrolyte," *Energy Storage Materials* 75 (2025): 104052.

168. S. He, Y. Chen, J. Fang, Y. Liu, and Z. Lin, "Optimizing Photocatalysis via Electron Spin Control," *Chemical Society Reviews* 54 (2025): 2154–2187.

169. A. A. B. Fauzi, N. Chitraningrum, I. Budiman, et al., "A State-of-The-Art Review on Lignocellulosic Biomass-Derived Activated Carbon for Adsorption and Photocatalytic Degradation of Pollutants: A Property and Mechanistic Study," *Environmental Science and Pollution Research* 31, no. 56 (2024): 64453–64475.

170. C. Zhu, Q. Fang, R. Liu, W. Dong, S. Song, and Y. Shen, "Insights Into the Crucial Role of Electron and Spin Structures in Heteroatom-Doped Covalent Triazine Frameworks for Removing Organic Micropollutants," *Environmental Science & Technology* 56, no. 10 (2022): 6699–6709.

171. L. Cheng, Y. Zhang, W. Fan, and Y. Ji, "Synergistic Adsorption-Photocatalysis for Dyes Removal by a Novel Biochar–Based Z-Scheme Heterojunction BC/2ZIS/WO_3: Mechanistic Investigation and Degradation Pathways," *Chemical Engineering Journal* 445 (2022): 136677.

172. L. Chen, X. Ding, Z. Wang, et al., "Advances in In Situ/Operando Techniques for Catalysis Research: Enhancing Insights and Discoveries," *Surface Science and Technology* 2, no. 1 (2024): 9.

173. H. Issa Hamoud, L. Wolski, I. Pankin, M. A. Bañares, M. Daturi, and M. El-Roz, "In Situ and Operando Spectroscopies in Photocatalysis: Powerful Techniques for a Better Understanding of the Performance and the Reaction Mechanism," *Topics in Current Chemistry* 380, no. 5 (2022): 37.

174. S. K. Tiwari, M. Bystrzejewski, A. De Adhikari, A. Huczko, and N. Wang, "Methods for the Conversion of Biomass Waste Into Value-Added Carbon Nanomaterials: Recent Progress and Applications," *Progress in Energy and Combustion Science* 92 (2022): 101023.

175. A. Arabpour, S. Dan, and H. Hashemipour, "Preparation and Optimization of Novel Graphene Oxide and Adsorption Isotherm Study of Methylene Blue," *Arabian Journal of Chemistry* 14, no. 3 (2021): 103003.

176. Q. Zaib and F. Ahmad, "Optimization of Carbon Nanotube Dispersions in Water Using Response Surface Methodology," *ACS Omega* 4, no. 1 (2019): 849–859.

177. J. H. Chung, H. Nur Hasyimah, and N. Hussein, "Application of Carbon Nanotubes (CNTs) for Remediation of Emerging Pollutants-A Review," *Tropical Aquatic and Soil Pollution* 2, no. 1 (2021): 13–26.

178. V. I. Isaeva, M. D. Vedenyapina, A. Y. Kurmysheva, et al., "Modern Carbon–Based Materials for Adsorptive Removal of Organic and Inorganic Pollutants From Water and Wastewater," *Molecules* 26, no. 21 (2021): 6628.

179. H.-J. Li, B.-W. Sun, L. Sui, D.-J. Qian, and M. Chen, "Preparation of Water-Dispersible Porous gC_3N_4 With Improved Photocatalytic Activity by Chemical Oxidation," *Physical Chemistry Chemical Physics* 17, no. 5 (2015): 3309–3315.

180. Z. Zhang, Y. Lu, Y. Zhao, L. Cui, C. Xu, and S. Wu, "Current Developments in Chitosan-Based Hydrogels for Water and Wastewater Treatment: A Comprehensive Review," *ChemistrySelect* 10, no. 6 (2025): e202404061.

181. S. Meropoulis and C. A. Aggelopoulos, "Advancing Nanopulsed Plasma Bubbles for the Degradation of Organic Pollutants in Water: From Lab to Pilot Scale," *Technologies* 12, no. 10 (2024): 189.

182. E. Lizundia, F. Luzi, and D. Puglia, "Organic Waste Valorisation Towards Circular and Sustainable Biocomposites," *Green Chemistry* 24, no. 14 (2022): 5429–5459.

183. S. Yu, J. He, Z. Zhang, et al., "Towards Negative Emissions: Hydrothermal Carbonization of Biomass for Sustainable Carbon Materials," *Advanced Materials* 36, no. 18 (2024): 2307412.

184. R. Sivaranjanee, P. S. Kumar, and G. Rangasamy, "A Recent Advancement on Hydrothermal Carbonization of Biomass to Produce Hydrochar for Pollution Control," *Carbon Letters* 33, no. 7 (2023): 1909–1933.

185. P. Rachitha, N. K. L. Gowda, N. Sagar, N. Sunayana, M. Uzma, and V. B. Raghavendra, *Risk Management, Regulatory Aspects, Environmental Challenges, and Future Perspectives of Functionalized Carbon Nanostructures, Handbook of Functionalized Carbon Nanostructures: From Synthesis Methods to Applications* (Springer, 2024), 2701–2742.

186. A. M. Shafi'i, Ma. A. Muhammad, M. Sulaiman, et al., "Carbon-Based Hybrid Materials in Water Treatment: Comprehensive Insights and Applications," *International Journal of Multidisciplinary Research* 2 no. 7 (2024): 90–119.

187. U. Meraj, E. Laiq, R. Bushra, et al., "Hydrothermal Synthesis of Okra Waste-Derived CQDs-CNTs Nanocomposites: Potent Catalysts for Pollutant Degradation of RhB and MO Dyes and Its Interaction With Lysozyme Protein," *Biomass Conversion and Biorefinery* 15 (2025): 20493–20513.

188. Y. Fang, Y. Tang, G. Li, et al., "Synergistic Adsorption Mechanisms of Self-N-Doped Biochar for Levofloxacin Elimination: Integrated Experimental and DFT Studies," *Environmental Research* 285 (2025): 122634.

189. T. N. Lotha, L. Rudithongru, V. Nakro, K. Ao, and L. Jamir, "Experimental and Theoretical Insights on Biomass-Derived Activated Carbon for the Removal of Aniline Blue and Malachite Green Dyes," *Biomass Conversion and Biorefinery* 15 (2025): 25591–25609.